Author Manuscript

Author Manuscript

Author Manuscript

Author Manuscript

HHS Public Access

Author manuscript

Biochemistry. Author manuscript; available in PMC 2017 November 16.

Published in final edited form as:

Biochemistry. 2014 December 23; 53(50): 7914–7928. doi:10.1021/bi501323h.

Pulse Electron Paramagnetic Resonance Studies of the Interaction of Methanol with the S_2 State of the Mn_4O_5Ca Cluster of Photosystem II

Paul H. Oyala[†], **Troy A. Stich**[†], **Jamie A. Stull**[†,§], **Fangting Yu**[‡], **Vincent L. Pecoraro**[‡], and **R. David Britt**[*,†]

[†]Department of Chemistry, University of California-Davis, One Shields Avenue, Davis, California 95616, United States

[‡]Department of Chemistry, University of Michigan, Ann Arbor, Michigan 41809, United States

[§]Los Alamos National Laboratory, Los Alamos, New Mexico 87545, United States

Abstract

The binding of the substrate analogue methanol to the catalytic Mn_4CaO_5 cluster of the water-oxidizing enzyme photosystem II is known to alter the electronic structure properties of the oxygen-evolving complex without retarding O_2-evolution under steady-state illumination conditions. We report the binding mode of ^{13}C-labeled methanol determined using 9.4 GHz (X-band) hyperfine sublevel-correlation (HYSCORE) and 34 GHz (Q-band) electron spin–echo electron nuclear double resonance (ESE-ENDOR) spectroscopies. These results are compared to analogous experiments on a mixed-valence Mn(III)Mn(IV) complex (2-OH-3,5-Cl_2-salpn)$_2$Mn(III)Mn-(IV) (salpn = *N*,*N*′-bis(3,5-dichlorosalicylidene)-1,3-diamino-2-hydroxypropane) in which methanol ligates to the Mn(III) ion (Larson et al. (1992) *J. Am. Chem. Soc.*, *114*, 6263). In the mixed-valence Mn(III,IV) complex, the hyperfine coupling to the ^{13}C of the bound methanol (A_{iso} = 0.65 MHz, T = 1.25 MHz) is appreciably larger than that observed for ^{13}C methanol associated with the Mn_4CaO_5 cluster poised in the S_2 state, where only a weak dipolar hyperfine interaction (A_{iso} = 0.05 MHz, T = 0.27 MHz) is observed. An evaluation of the ^{13}C hyperfine interaction using the X-ray structure coordinates of the Mn_4CaO_5 cluster indicates that methanol does not bind as a terminal ligand to any of the manganese ions in the oxygen-evolving complex. We favor methanol binding in place of a water ligand to the Ca^{2+} in the Mn_4CaO_5 cluster or in place of one of the waters that form hydrogen bonds with the oxygen bridges of the cluster.

Graphical Abstract

[*]Corresponding Author: rdbritt@ucdavis.edu.

Notes

The authors declare no competing financial interest.

Supporting Information

Supplementary Figures S1–S10 containing additional EPR spectra and isosurface plots. This material is available free of charge via the Internet at http://pubs.acs.org.

Author Manuscript Author Manuscript Author Manuscript Author Manuscript

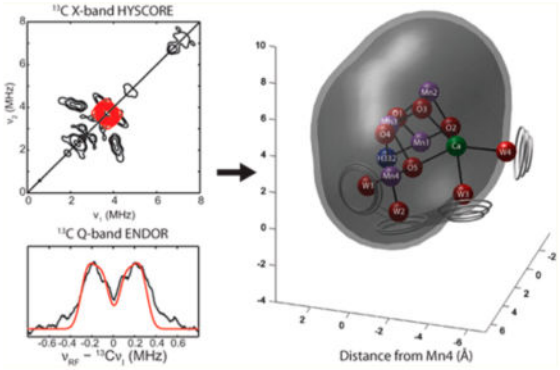

Photosystem II (PSII) is a membrane-spanning protein complex residing in the thylakoid membrane of oxygenic photosynthetic organisms.[2–4] PSII splits water into protons and molecular oxygen through a series of light-induced electron transfer events.[5] This light-driven oxidation of water is catalyzed by the oxygen-evolving complex (OEC), a Mn_4CaO_5 cluster that cycles through a five-step redox cycle as electrons are successively abstracted from the cluster via a transient neutral tyrosine radical $Y_Z^{\bullet}$ (D1-Y161) generated by the chlorophyll-based photo-oxidant P_{680}^{+}.[5] The intermediate redox states of this cycle are denoted as S_0–S_4 in order of increasing net oxidation state, with S_1 being the dark-stable state.[6] Once the S_4 state is achieved, the OEC recycles rapidly to S_0, and dioxygen is formed and released. The resultant protons are released on the electron donor side of the membrane, while the electrons are transferred across the thylakoid membrane to reduce plastoquinone to plastoquinol. The Mn_4CaO_5 cluster itself is comprised of a μ-oxido-bridged cuboidal Mn_3CaO_4 unit containing Mn1–3, with the fourth "dangler" Mn (Mn4) linked to the cuboidal subunit via O4 and O5 (atom numbering shown in Figure 1A[2]). The cluster is also bound to the PSII proteins via six carboxylate ligands from the D1 and CP43 subunits of PSII, and one histidine, D1-His332.[2,7] The individual Mn ions of the cluster experience changes in oxidation state with each S state transition. In the well characterized S_2 state, the oxidation states of the four manganese ions are generally considered to be III, IV, IV, IV.[8–11] Multifrequency electron spin–echo envelope modulation (ESEEM) spectroscopic measurements of the magnitude of the nitrogen hyperfine interaction (HFI) from His332, the only nitrogenous ligand to Mn in the Mn_4CaO_5 cluster, show that in the spin $S = 1/2$ conformation of the S_2 state the sole Mn(III) ion is in the Mn1 position.[7]

Because the substrate of the OEC is water, analysis of water interactions with the OEC is complicated, as true substrate waters must be differentiated from additional ligand and matrix waters that are not directly involved in water oxidation. To this end, the interactions of the OEC with small molecule analogues to water, such as small amines,[10,13–26] hydrazine,[25,26] hydrogen peroxide,[27–29] and several primary alcohols[19,22,30–40] have been used to build a better picture of the substrate binding modes.

Methanol has been shown to affect the EPR spectra of many of the oxidation states of the OEC and has been proposed to bind to the cluster by coordinating to one or more of the Mn ions.[30,32–37] The presence of methanol changes the shape and/or intensity of almost all continuous-wave electron paramagnetic resonance (CW EPR) spectroscopic signals of the

Author Manuscript Author Manuscript Author Manuscript Author Manuscript

OEC, including the S_0 (spin $S = 1/2$) multiline[33,36,41–47] and S_2($S = 1/2$) multiline signal,[11,31–33,48,49] the two parallel-mode signals of the S_1 state of higher plants ($S = 1$)[50,51] and cyanobacteria ($S = 2$),[52] and the split signals that result from coupling of the $Y_z^{\bullet}$ radical to the paramagnetic forms of S_0, S_1, and S_3.[35] There appear to be differences in the concentration dependence of the effects of methanol on these signals that are S-state dependent, indicating that the binding affinity of MeOH at the Mn_4CaO_5 cluster may change as a function of the oxidation state of the cluster.[34]

While the S_2 state typically exhibits an EPR multiline (MLS) signal at $g = 2$ arising from an $S = 1/2$ species, higher spin signals at $g \geq 4.1$ arising from a high-spin ($S = 5/2$)[53] conformation of the Mn_4CaO_5 cluster are also observed under a variety of sample conditions.[10,54–57] In the presence of methanol and other primary alcohols, the equilibrium between these two forms of S_2 is shifted in favor of the $S = 1/2$, $g = 2$, MLS signal.[31] A recent study by Sjöholm et al. showed that methanol-induced changes in the $S_1Y_z^{\bullet}$ split signal have a different concentration dependence than what is observed for the $S_2Y_z^{\bullet}$ signal (both induced from samples initially poised in the S_2 state). This was interpreted as evidence for the existence of two binding sites for methanol at the Mn_4CaO_5 cluster in the S_2 state, with one having a higher affinity ($[MeOH]_{1/2}$ = 0.10% (v/v)) and one with a lower affinity ($[MeOH]_{1/2}$ = 0.28 (v/v)), where the $[MeOH]_{1/2}$ values represent the half-saturation value of methanol concentration for these two sites.[34] These values are similar to the methanol binding affinity for the S_2 state ($[MeOH]_{1/2}$ = 0.32% (v/v)) first estimated by Force and coworkers from analysis of concentration dependence of the deuterium ESEEM spectroscopy in samples treated with CD_3OH (D = ^{2}H).[31]

Another effect that methanol has on the S_2 state of the Mn_4CaO_5 is to increase the energy separation (Δ) between the lowest-energy spin manifold ($S = 1/2$) of the low-spin form of S_2 and the first, higher-energy manifold ($S = 3/2$).[19,32] This increase in Δ reduces the anisotropy of the ^{55}Mn HFI tensors owing to a diminished relative contribution from the Mn(III) ZFS. This reduced ^{55}Mn HFI anisotropy leads to an observed narrowing of the S_2 MLS CW EPR signal.[32,33] Su and co-workers utilized a simplified spin-coupling model of the S_2 state in which the relative energies of the spin manifolds of the $S = 1/2$ ground state are proportional to a single effective coupling constant J_{eff} (with $\Delta = 3/2J_{eff}$), which represents the coupling between the monomeric "dangler" Mn4 ($S = 3/2$) and the $CaMn_3$ cluster (in either the $S = 1$ or 2 state).[32] Thus, the increase in Δ upon MeOH addition arises from an increase in J_{eff}. Interestingly, the magnitude of the change in Δ due to methanol seems to be much smaller in PSII cores purified from the thermophilic cyanobacterium *Thermosynechococcus elongatus* (*T. elongatus*) in comparison to PSII from higher plants.[32] This difference may due to Δ being intrinsically higher in the PSII preparations from *T. elongatus*, thus mitigating the effect of methanol binding to the cluster, rather than a difference in the binding mode of methanol to the cluster.

Though methanol seems likely to compete with water for binding to the OEC, it is not inhibitory to oxygen evolution up to a concentration of 3 M and then only inhibits activity by 10% at a concentration of 5 M.[31] However, these studies were performed under saturating white-light illumination conditions under which PSII turnover is likely limited at the acceptor side by the rate of plastiquinone/quinol exchange at the Q_B binding site.[37] Flash-

Author Manuscript Author Manuscript Author Manuscript Author Manuscript

induced O_2-evolution pattern (FIOP) measurements have shown that the miss parameter, α, for S_i state advancement has a linear dependence on methanol concentration in the range of 0–10% (v/v),[37] indicating that methanol may bind with a similar affinity as water at one or more of the substrate sites. Isotopically labeled small alcohols such as methanol can serve as a probe for EPR spectroscopy as magnetic nuclei unique to the substrate analogue can be introduced. Previous EPR spectroscopic work probed methanol binding using CD_3OH via X-band ESEEM spectroscopy and measured deuteron couplings to the S_2 state consistent with direct ligation of methanol to the OEC, possibly through coordination as a terminal ligand to Mn.[31,51] The use here of ^{13}C-methanol (nuclear spin $I = 1/2$) offers an additional, potentially more specific probe of the location of the methyl group due to the presence of only a single magnetic nucleus that is one bond closer to the paramagnetic system. In this study, we employed pulse EPR spectroscopy to measure the hyperfine coupling between the ^{13}C of the methyl group of methanol and the $S = 1/2$ form of the S_2 state of the OEC in order to evaluate possible methanol binding sites.

Synthetic mixed-valence multinuclear manganese complexes are often invoked as spectroscopic and structural models for multinuclear manganese active sites in enzymes such as manganese catalase and the OEC of PSII. Previously, methanol and water ligation to the dinuclear Mn complex (2-OH-3,5-Cl_2-salpn)$_2$Mn(III)Mn(IV),[1] (Mn(III,IV)salpn), (salpn = *N,N′*-bis(3,5-dichlorosalicylidene)-1,3-diamino-2-hydroxypropane) (heretofore referred to as Mn(III,IV)salpn) was investigated using deuterated and proteated methanol and water.[30] In solutions containing Mn(III,IV)salpn and an electron-donating solvent such as water, tetrahydrofuran (THF), or methanol, the solvent binds directly to the Mn(III) ion along the Jahn–Teller elongated axis to form Mn(III,IV)salpn + ligand (see Figure 1B) and causes a loss of molecular symmetry by rendering one of the two μ-alkoxido bridges monodentate. Herein, we have performed pulse EPR experiments on Mn(III,IV)salpn + ^{13}C-methanol in order to determine the magnitude of ^{13}C-coupling arising from methanol bound to Mn(III) in exchange-coupled systems consisting of antiferromagnetically coupled Mn(III) and Mn(IV). This coupling in the synthetic system is likely to approximate the upper bound of ^{13}C couplings that one could expect to observe from ^{13}C MeOH bound to the S_2 state.[7,10,11,58]

MATERIALS AND METHODS

Mn(III,IV)salpn Sample Preparation

Mn(III,IV)salpn + methanol samples were prepared by methods described previously using ^{13}C-methanol (99%, Cambridge Isotope Laboratories) or natural-abundance methanol (Fisher). The final concentration of Mn(III,IV)salpn in all samples was 2 mM, while the concentration of methanol was ≥1 M. After preparation, samples were placed in 3.8 mm O.D. precision quartz EPR tubes for X-band EPR experiments, and 2.4 mm O.D. tubes for Q-band experiments. Successful complexation by methanol was judged on the basis of the appearance of the 12-line CW EPR spectrum that is diagnostic of the solvent-bound asymmetric form.[1]

Author Manuscript Author Manuscript Author Manuscript Author Manuscript

PSII Sample Preparation

PSII-enriched membranes from market-fresh spinach were purified according to the method of Berthold, Babcock, and Yocum[59] modified to remove adventitiously bound Mn(II) using 5 mM $CaCl_2$ and 1 mM EDTA.[60,61] Artificial electron acceptor phenyl-*p*-benzoquinone (PPBQ) was added from a 250 mM stock in DMSO to a final concentration of 1 mM. ^{13}C-labeled or natural abundance methanol was added to the final resuspension buffer to either 0.5 or 5% (v/v). Membranes were centrifuged for 20 min at 30000*g*, and the final pellet was loaded into 3.8 mm O.D. precision quartz EPR tubes for X-band EPR experiments, and 2.4 mm O.D. tubes for Q-band experiments. To observe the S_2 multiline signal, samples were illuminated for 8 min at 205 K using a liquid nitrogen-cooled gas-flow apparatus and a Sylvania ELH 300 W halogen-tungsten lamp (color temperature = 3350 K).

EPR Spectroscopy

X-Band CW EPR—All CW EPR spectra were collected at the specified temperature using a Bruker ELEXSYS E500 X-band spectrometer equipped with an Oxford Instruments ESR900 cryostat and an ITC-503 temperature controller.

Pulse EPR and ENDOR—All pulse EPR and electron–nuclear double resonance (ENDOR) spectroscopic studies were performed at 4.5 K using a Bruker ELEXSYS E580 pulse EPR spectrometer equipped with an Oxford-CF935 liquid helium cryostat and an ITC-503 temperature controller. X-band hyperfine sublevel-correlation (HYSCORE) spectroscopy was performed with a Bruker MS-5 resonator using the pulse sequence: $\pi/2$-τ-$\pi/2$-T_1-π-T_2-$\pi/2$-echo. Q-band pulse EPR and Mims ENDOR was performed using the same E580 EPR spectrometer equipped with a 1 KW ENI amplifier and an R.A. Isaacson-designed cylindrical TE011 resonator[62] adapted from previous use for pulse EPR in an Oxford Instruments CF935 cryostat. Q-band electron spin–echo (ESE) detected EPR spectra were collected using the sequence $\pi/2$-τ-π-echo, and Q-band Mims ENDOR spectra were acquired using the pulse sequence $\pi/2$-τ-$\pi/2$-π_{RF}-$\pi/2$-echo. Specific parameters for field positions, microwave frequencies, pulse and delay lengths are given in the captions of each figure. For PSII pulse EPR experiments, all spectra were acquired at a field position corresponding to $g = 1.98$, near the maximum of the S_2 MLS signal, yet not overlapping with the EPR spectrum of the persistent tyrosine radical $Y_D^{\bullet}$.

HYSCORE/Mims ENDOR Simulations

All pulsed EPR spectra were fit assuming an effective spin $S = 1/2$ ground state (see Theory section, The Spin Hamiltonian Formalism), and the hyperfine terms were treated using second order perturbation theory. The hyperfine tensor parameters were determined using a least-squares fitting algorithm of the experimental spectra. The best fits in these cases were typically roughly axial in symmetry. In all cases, introducing additional asymmetry resulted in much poorer matches to the experimental data. The S_2 EPR signal has an approximately isotropic *g*-tensor, and the spectrum is broadened by the ^{55}Mn HFI from the four Mn nuclei to approximately 180 mT. As a result of this hyperfine broadening, it is unfeasible to achieve significant orientation selection, especially at the center of the spectrum, where these experiments were performed. Thus, changing the orientation of the hyperfine tensor

Author Manuscript Author Manuscript Author Manuscript Author Manuscript

orientation relative to the *g*-tensor produces no significant change in the simulated spectrum for the weak coupling of the ^{13}C to the S_2 state. Therefore, the simulations were performed with all tensors aligned colinearly. Spectral simulations were performed using MATLAB 7.8.0 (R2009a) software package (The Mathworks Inc., Natick, MA) using the EasySpin 4.5.5 toolbox.[63,64] It should be noted that this simulation suite takes into account and reproduces the tau-dependent suppression that modifies the spectral lineshapes observed for Mims ENDOR,[63,64] in which the intensity of peaks are modulated with the envelope of $\sin^2(A\tau/2)$, where A is the hyperfine coupling for a given nucleus and orientation of the spin system.[65] Approximate error estimates for simulated hyperfine values were determined by visual inspection of spectral fit as the hyperfine was varied from the best fit.

THEORY

The Spin Hamiltonian Formalism

Both species considered in this report—the Mn (III,IV)salpn dimer and the S_2 state of the OEC—are composed of high-spin Mn(III) and Mn(IV) ions that are exchange-coupled to give a net $S = 1/2$ spin system.[5,66,67] The following uncoupled spin Hamiltonian is used to show how the intrinsic site-specific magnetic properties of each of the paramagnetic Mn ions can be added together to give the magnetic behavior of the total exchange-coupled spin system.

$$\hat{H}=\sum_{i}^{n}\sum_{j}^{m}[\mu_{\mathrm{B}}\ \vec{B_0}\ g_i\hat{S}_i+\mu_{\mathrm{N}}g_{\mathrm{N},j}\ \vec{B_0}\ \hat{I}_j+\hat{S}_iA_{ij}\hat{I}_j+\hat{S}_iD_i\hat{S}_i+\hat{I}_jP_j\hat{I}_j]-\sum_{i>k}^{n}\hat{S}_iJ_{ik}\hat{S}_k \quad (1)$$

These terms are, in order: the electron and nuclear Zeeman interactions of the electron spin of site *i* and nuclear spin center *j* with the applied magnetic field B_0; the hyperfine interaction (HFI) (A) that couples each electron and nuclear spin; the zero-field splitting (ZFS) tensor (D); the nuclear quadrupole tensor (P); and the Heisenberg–Dirac–van Vleck exchange term (J), a pairwise exchange coupling term (often approximated as being isotropic) between different paramagnetic centers in the spin system.

When these exchange interactions are sufficiently strong, all of the electron spin momenta can couple to produce a new manifold of possible spin states S. Each of those spin states can be described by an effective or molecular spin Hamiltonian such as the one shown below for the $S = 1/2$ spin systems studied here:

$$\hat{H}=\mu_0\ \vec{B_0}\ g_{\mathrm{eff}}\hat{S}+\sum_{j}^{m}[\hat{S}A_{\mathrm{eff,j}}\hat{I}_j+\hat{I}_jP_j\hat{I}_j+\mu_{\mathrm{N}}g_{\mathrm{N}}\ \vec{B_0}\ \hat{I}_j] \quad (2)$$

In this representation, g_{eff} is the observed *g*-matrix, and $A_{\mathrm{eff},j}$ is the observed HFI for every nucleus *j* in the spin system. These measured *g*-values and hyperfine parameters are related to the intrinsic magnetic parameters described in eq 1 by projection factors ρ_i for each spin center in the complex. These projection factors, or Clebsch-Gordan coefficients, relate the

Author Manuscript Author Manuscript Author Manuscript Author Manuscript

uncoupled angular momentum tensors of each spin center to the new total electron spin vector and can be calculated following the methodology outlined in Chapter 3 of Bencini and Gatteschi.[57] The projection factors can be affected by covalency and by the site-specific zero-field splitting tensor D_i for each coupled ion if the J/D ratio is small.[68] Thus, to determine precisely what the true projection factor is, one needs to measure the metal HFI of the coupled system and compare it to mononuclear standards.[10,69]

Once the projection factors are known, the measured HFI elements $A_{\mathrm{eff},j}$ can be interpreted in terms of covalency and interspin distance (vide infra). The site-specific hyperfine tensor (A_j) can be decomposed into an isotropic component (A_{iso}) stemming from unpaired electron spin in s-orbitals of the atoms containing magnetic nuclei and a dipolar coupling tensor (T) due to the through-space interaction between the electron and nuclear spins. The total hyperfine interaction is written as

$$[A_x, A_y, A_z] = [A_{\mathrm{iso}} - T, A_{\mathrm{iso}} - T, A_{\mathrm{iso}} + 2T] \quad (3)$$

In the spin-only point-dipole approximation, where g-matrix anisotropy is ignored and the center of unpaired electron density and the magnetic nucleus are suitably distant from each other ($r > 2.5$ Å), T is simply:

$$T = \frac{\mu_0}{4\pi\hbar} g_{\mathrm{ave}} \mu_{\mathrm{B}} g_{\mathrm{N}} \mu_{\mathrm{N}} \rho \left(\frac{3\cos^2\theta - 1}{r^3} \right) \quad (4)$$

The distance between the electron and nuclear spin is represented by r, the angle between this vector and the applied magnetic field $\vec{B}_0$ is defined as θ and the unpaired spin population on the specified spin center is given by ρ. Values for T can be computed for the nucleus interacting with each spin center using eq 4. This can be converted into a vector of the form $[-T, -T, +2T]$ and scaled by the appropriate projection factor. These pairwise dipolar interactions must be rotationally transformed into a common axis system before being added together to give the cluster-wide dipolar hyperfine coupling term for the nucleus.

RESULTS AND DISCUSSION

X-Band and Q-Band ESE-EPR of Methanol-Ligated Mn(III,IV)salpn

The X- and Q-band two-pulse ESE field-swept EPR spectra and pseudomodulated[70] spectra of Mn-(III,IV)salpn + ^{13}C-methanol are presented in Figure 2. The X-band data match well with previously published spectra,[1,10,30] with at least 12 resolved peaks[68,71–73] that are diagnostic of the effective $S = 1/2$ electron spin coupled to two inequivalent ^{55}Mn ($I = 5/2$) nuclei.

At Q-band, a loss of resolved ^{55}Mn HFI splittings is observed owing to the significant g-anisotropy present for Mn(III,IV)-salpn which leads to a spreading of the EPR spectrum

Author Manuscript Author Manuscript Author Manuscript Author Manuscript

over a larger field range with increasing the resonant excitation frequency. Interference of the overlapping ^{55}Mn hyperfine patterns for each discrete powder pattern and g-strain may also contribute to the loss of resolved structure at higher frequency.

X-Band HYSCORE of Mn(III,IV)salpn + ^{13}C Methanol

Field-dependent X-band HYSCORE spectroscopy was performed on the Mn(III,IV)salpn adduct with both ^{13}C-labeled (see Figure 3) and natural-abundance methanol (see Supporting Information (SI) Figure S2). At each field position for Mn(III,IV)salpn + ^{13}C methanol, clear correlation ridges centered at the ^{13}C Larmor frequency are evident in the + + quadrant. These correlation ridges are absent in the natural-abundance samples (SI Figure S2).

These signals are well simulated by a moderate coupling where A_{iso} = 0.65 ± 0.05 MHz and T = 1.25 ± 0.05 MHz. The degree of curvature of the correlation ridge is diagnostic of a rather large anisotropic HFI,[74] consistent with the assignment of $T > A_{iso}$. The nonzero value for A_{iso} requires that there is some localization of unpaired electron density directly on the ^{13}C nucleus (see Theory section, The Spin Hamiltonian Formalism), suggesting that the corresponding ^{13}C methanol is directly ligated to a spin-carrying center (i.e., Mn) through the oxygen, as is expected from the crystal structure which establishes that methanol adduct binds to the Mn(III) ion.[1]

Q-Band Mims ENDOR of Mn(III,IV)salpn + ^{13}C Methanol

Q-band Mims ENDOR spectra acquired at three different field positions are presented in Figure 4. Spectra were acquired using three different tau values (300, 500, and 800 ns) at each field in order to ensure that tau-dependent blind-spots did not bias simulations. As compared to the HYSCORE method, Mims ENDOR spectroscopy is more sensitive to extremely weak nuclear couplings. Because of this increased sensitivity, a new, weaker class of ^{13}C-coupled nuclei was detected in addition to that observed in the corresponding HYSCORE spectra (Figure 3). The ENDOR spectral features arising from this weak class are well-simulated using the parameters A_{iso} = 0.03 ± 0.02 MHz and T = 0.12 ± 0.04 MHz. We attribute these features to distant, nonbonded matrix ^{13}C-methanol. The higher relative intensity of the matrix peaks is rationalized by the approximately 500-fold excess of ^{13}C-methanol in the sample compared to concentration of Mn(III,IV)salpn, meaning that several second solvation shell methanol molecules would be expected to interact with each Mn(III,IV)salpn. This matrix contribution was similarly seen in the previous ESE-ENDOR and ESEEM spectroscopic studies conducted using CD_3OH.[30] The ENDOR features of the more strongly coupled class of ^{13}C nuclei was modeled using the same parameters employed in the HYSCORE simulation (Table 1). Our two-component simulation utilizes a 10:1 ratio of “matrix” ^{13}C to “bound” ^{13}C, which is consistent with the previous study by Randall et al. in which a 30:1 ratio was used to fit the deuterium ESEEM.[30] The large anisotropy of the more strongly coupled ^{13}C HFI is indicated by the field-dependent changes in the observed spectra.

Author Manuscript Author Manuscript Author Manuscript Author Manuscript

Mn(III,IV)salpn Dipolar HFI Isosurface Plot

Using the observed dipolar ^{13}C HFI (T) for methanol directly bound to Mn(III,IV)salpn (1.25 MHz), the atomic coordinates from the crystal structure Mn(III,IV)salpn + THF, and the methodology for computing the distance of a nucleus from the Mn(III) of the Mn(III,IV) dimer developed previously,[30,75] an isosurface plot was constructed representing a three-dimensional map of the possible locations of the ^{13}C nucleus with reference to the crystal structure coordinates. In the strong-exchange limit where $J/D \gg 1$, the spin projection factors for high-spin Mn(III) and Mn(IV) are +2 and −1, respectively.[68] In the case of Mn(III,IV)salpn, the single alkoxido bridge between the Mn(III) and Mn(IV) ions produces a fairly small J, estimated to be 10 cm^{-1}.[1] For high-spin Mn(III), the magnitude of D is typically between 1 to 5 cm^{-1}; thus the strong exchange limit is not explicitly met.[76] Because of this, the effective ^{55}Mn HFI should be divided by the range of intrinsic ^{55}Mn hyperfine values in the literature for mononuclear Mn(III) and Mn(IV) compounds to come up with an estimate for the range of spin projection factors for each Mn ion within Mn(III,IV)salpn.[10] Previous ^{55}Mn ENDOR spectroscopic studies of Mn(III,IV)-salpn + THF estimated A_{iso} as −337 and 197 MHz for the Mn(III) and Mn(IV) ions, respectively.[10] Dividing these values by the range of intrinsic ^{55}Mn HFI values for mononuclear standards, the range of isotropic projection values for these ions is −1.5 to −2 for the Mn(III) ion, and 0.78 to 1.05 for the Mn(IV) ion.

In addition to constructing a surface based on the observed ^{13}C HFI, realistic distributions of the position of the ^{13}C-methanol must be considered based on known Mn–O—C bond angles. To this end, a search of the Cambridge Crystallographic Data Centre (CCDC) database for reported crystal structures with methanol directly ligated to manganese yielded the upper[77] and lower[78] bounds (3.529 and 3.120 Å, respectively) for observed Mn····C distances in the literature and an average value of (3.299 Å). In this model of the methanol-bound Mn(III,IV)salpn, the position of the oxygen atom of methanol was assumed to be identical to that determined for the oxygen atom of THF by X-ray crystallographic analysis. Using this method, the likely position of the carbon of methanol was determined and is represented by the gray rings in Figure 5. Inspection of the isosurface plot for T = 1.25 MHz shows overlap of the likely position of the methanol carbon determined using geometry considerations constrained by entries in the CCDC and its position determined using the dipolar HFI. Considering the increased steric bulk of THF compared to methanol, perhaps methanol can bind somewhat closer to the Mn(III) than what is shown in our model. Indeed, shortening the Mn–O bond length by 0.1 Å produces an even better match of these radial distributions with the observed ^{13}C dipolar HFI isosurfaces. Using this validated spectrostructural approach, the binding site of methanol in PSII will now be examined.

X-Band HYSCORE of the S_2 State of the OEC + ^{13}C-Methanol

X-band HYSCORE spectra of the S_2 state of PSII in the presence of 5% (v/v) (1.24 M) ^{13}C methanol, 0.5% (v/v) (124 mM) ^{13}C methanol, and natural-abundance methanol are presented in Figure 6.

In contrast to Mn(III,IV)salpn, X-band HYSCORE spectra of PSII in the S_2 state in the presence of both 5% and 0.5% ^{13}C-methanol show a weak ^{13}C coupling that is not

Author Manuscript Author Manuscript Author Manuscript Author Manuscript

adequately resolved by X-band HYSCORE spectroscopy for quantitative determination of the magnitude of the coupling. The increased relative intensity of the ^{13}C signal in the presence of 5% ^{13}C methanol is likely due to the interaction between matrix methanol with paramagnetic contaminants, such as adventitiously bound Mn(II) and Cu(II). This signal is completely absent in the PSII sample treated with 5% (v/v) natural abundance methanol. The other signals that are evident in all HYSCORE spectra arise from the strongly coupled ^{14}N nucleus in histidine 332, a ligand to Mn1. These ^{14}N signals are well simulated using parameters from a multifrequency ESEEM study by Stich et al.: A_{iso} = 6.95 MHz; A_{aniso} = [0.2, 1.3, −1.5] MHz; e^2Qq/h = 1.98 MHz; η = 0.82.[7] For full HYSCORE spectra and simulations of ^{13}C and ^{14}N signals, see SI, Figure S4.

Q-Band Mims ENDOR of the S_2 State of the OEC + 5% and 0.5% ^{13}C-Methanol

In order to attain a quantitative measurement of the weak ^{13}C couplings arising from the interaction of methanol with the OEC, the more sensitive Mims ENDOR method at Q-band was utilized. Dark-subtracted Mims ENDOR spectra of S_2 in the presence of 5% (v/v) (1.24 M) and 0.5% (v/v) (124 mM) are shown in Figure 7.

As was observed in the X-band HYSCORE spectrum, the spectra acquired of samples with 5% (v/v) ^{13}C methanol display considerable signal in the dark-adapted Mims ENDOR spectra (see SI Figure S5), likely due to the interaction between matrix methanol with paramagnetic contaminants, such as adventitiously bound Mn(II) and Cu(II). Subtractions were performed by scaling the respective dark-adapted and illuminated ENDOR spectra by the number of scans acquired and the echo intensity of the ESE-EPR spectrum obtained using the same microwave pulse sequence as was used to acquire the ENDOR spectrum. For the 0.5% (v/v) sample, there was essentially no signal observed in the dark-adapted spectra, but the illuminated spectra show the same weak ^{13}C coupling that is evident at 10 times that concentration. These ENDOR spectra were simulated using a least-squares optimization routine and yielded a best fit of A_{iso} = 0.05 MHz ± 0.02 MHz and T = 0.27 ± 0.05 MHz. It should be noted that there appears to be only a single class of ^{13}C coupling resolved at both concentrations. This is notable given the findings of Sjöholm et al. that there are two binding sites for methanol to the S_2 state ($[MeOH]_{1/2}$ = 0.10%, 0.28%, respectively),[34] both of which should be saturated at the ^{13}C MeOH concentrations used for this study. It is possible that the two binding sites are both represented in these data but result in very similar small ^{13}C couplings that we are unable to differentiate in the ^{13}C ENDOR spectra. Interestingly, in a similar excess of ^{13}C methanol to that in the Mn(III,IV)salpn samples, there is no evidence for significant amounts of “matrix” methanol as is observed for the model complex. This is in agreement with previous ESEEM spectroscopic studies using CD_3OH[31] and indicates that there is limited access for methanol to the second coordination sphere of the Mn_4CaO_5 cluster.

The ^{13}C couplings observed for methanol-treated Mn-(III,IV)salpn and the methanol-treated OEC poised in the S_2 state are presented in Table 1. The nearly negligible isotropic ^{13}C HFI for methanol bound to the OEC—in contrast to A_{iso} = 0.65 MHz observed for methanol bound to Mn(III,IV)salpn—indicates that it is not binding along the Jahn–Teller axis of the lone Mn(III) of the S_2 state. Further, the small dipolar coupling (T) observed for the OEC-

Author Manuscript Author Manuscript Author Manuscript Author Manuscript

bound methanol suggests that the corresponding methyl group is not part of a ligand to a spin-bearing manganese center. From this, we conclude that methanol is not binding as a terminal ligand to any of the manganese ions in the OEC in the S_2 state.

An alternative mode for binding that could result in the very small observed ^{13}C HFI is the displacement of one of the μ-oxido bridges between two of the antiferromagnetically coupled Mn(IV) ions in the OEC. This positioning could conceivably give rise to a net projection factor of approximately zero and lead to a HFI value of nearly zero. The two most likely sites for μ-oxido binding of methanol to the OEC that could result in this net near-zero projection factor condition are the bridges between Mn4 and Mn3 (O4 and O5, Figure 1A) which effectively join the dangler Mn to the cuboidal Mn_3O_4Ca subunit. O5 is particularly interesting to consider, as it has been identified through ^{17}O EDNMR (electron–electron double resonance-detected nuclear magnetic resonance) spectroscopy to be capable of relatively rapid exchange (less than 15 s) with bulk water.[80] O5 has increasingly been invoked as being involved in O–O bond formation,[81] and as such competition with methanol could produce the observed increase in the miss factor for S-state turnover. However, displacement of O5 by methanol would place the methyl group within 2.5 Å of Mn1—the lone Mn(III)—which would dominate the effective spin projection factor at the ^{13}C nucleus. The estimated dipolar HFI for this orientation is ~1.6–2.3 MHz, which is much larger than what is observed by HYSCORE and ENDOR spectroscopy. Replacement of O4 by methanol would position the methyl group distal to the rest of the spin-carrying Mn ions in the OEC, presumably resulting in a very small effective ^{13}C HFI. However, in this scenario, the deuteron HFI of CD_3OH would be equally diminished, which does not match previously reported values determined from ESEEM spectroscopic studies.[31,47] One would also expect that replacing a μ-oxido bridge with a less electron-donating methoxy group would decrease the antiferromagnetic coupling between the adjacent spin centers, as has been observed for model complexes with successively protonated oxido-bridges or added μ-acetato bridges between manganese ions.[82,83] This is opposite of the observed effect of methanol on the separation of the ground state and first excited state of the S_2 state.[32] For these reasons, we now consider a model in which methanol instead displaces one or more of the two ligand waters of the Ca^{2+} ion of OEC (W3 and W4, Figure 1A).

PSII S_2 State Dipolar HFI Isosurface Plot Analysis

To further evaluate the potential for displacement by methanol for either of the two Ca-bound waters identified in the 1.9 Å crystal structure,[2] we again use the isosurface plots described above, this time generated using projection factors relevant for the low-spin S_2 state of the OEC. The equations for using the observed dipolar HFI to calculate the position of the ^{13}C nucleus must be extended to all four spin-carrying Mn centers,[31,75] using isotropic projection factors estimated from the ^{55}Mn isotropic HFI values for the S_2 state of the OEC reported previously[11] (see Table 2) and ranges of intrinsic ^{55}Mn HFI values reported in the literature for Mn(III) and Mn(IV).[76] Though the entire range of estimated projection factors is presented in Table 2, it must be noted that the upper limits of these values predict ligand HFI that are much more plausible and consistent with recent experimental findings. In particular, the measured coupling of the δ-nitrogen of D1-H332, when scaled by the projection factor value of 1.81, is consistent with the intrinsic histidine

Author Manuscript Author Manuscript Author Manuscript Author Manuscript

nitrogen–Mn(III) HFI determined in an earlier study of the dimanganese catalase.[7,84,85] Nonetheless, presented in Figure 8 are the isosurface plots of the potential location of the ^{13}C nucleus of methanol using both the upper and lower bounds of the estimated isotropic projection factors for each Mn ion in the OEC poised in the S_2 state.

The radial distributions (light gray rings, Figure 8) of likely positions of the methyl carbon of metal-bound methanol are centered about the oxygen atoms for each of the crystallographically identified ligand waters to the Mn_4CaO_5 cluster. For this model, the Mn–O bond lengths for the terminal water ligands to Mn4 (W1 and W2) have been adjusted to 2.0 Å (from 2.22 and 2.08 Å, respectively), as this is the typical Mn–O bond length for H_2O ligands to Mn(IV) observed in model compounds.[86–88] For methanol bound to Mn4, the same upper and lower bounds of bond angles and distances were used as was done in the analysis of Mn(III,IV)salpn. In the case of Ca-bound methanol, another search of the CCDC database for reported crystal structures with methanol directly ligated to Ca yielded upper[89] and lower bounds[90] (3.67 and 3.29 Å, respectively) and an average value (3.45 Å) for observed Ca····C distances.

In the interest of clarifying the potential overlap of the ^{13}C HFI isosurfaces with these radial distributions, the W1–Mn4–W2 and W3–Ca–W4 plane slices of the model presented in Figure 8 are shown in Figure 9.

In a manner consistent with the simple analysis of the magnitude of the ^{13}C coupling presented above, these plots confirm our previous conclusion that the Mn-bound waters (W1 and W2) are poor candidates for displacement by methanol, as the Mn····C distances that would result fall at least 0.5 Å short of the distances predicted from the dipolar ^{13}C HFI. Using this spectrostructural method, we conclude that methanol could be displacing the Ca-ligand W3, since for this site the observed ^{13}C dipolar hyperfine isosurface plot matches the geometrically constrained locations for the methyl group. This is the only OEC-bound water site identified in the Shen crystal structure that matches the experimentally determined ^{13}C HFI coupling. Supporting this view, ab initio calculations have suggested that the binding affinity of water to calcium is very similar to that of methanol to calcium, so facile substitution would be expected.[91,92] Models of the methanol-bound OEC with methanol binding in place of W3 also predict positions of the methyl deuterons which match reasonably well with the previous ESEEM spectroscopic results obtained using CD_3OH by Force et al. (see SI Figure S9).[31] Computational analysis performed by Ho and co-workers evaluating potential access channels for MeOH to the Mn_4CaO_5 cluster using the crystal structure published by Loll and co-workers,[4] as well as that of Ferreira et al.,[3] also indicate that the waters bound to the Ca^{2+} should be accessible to displacement by MeOH.[38] Binding of methanol at calcium is also potentially supported by the observation by Lohmiller et al. that removal of Ca^{2+} in PSII from spinach results in a loss of sensitivity of the modified S_2 multiline signal to the presence of methanol even though the overall structure of the remaining OEC is relatively unchanged.[39] However, it should be noted that the removal of Ca^{2+} also results in a change in ^{55}Mn couplings that is consistent with an increase in Δ similar to the effect of methanol, which may have prevented observation of changes in the ^{55}Mn ENDOR spectra due to treatment with methanol.[39]

Author Manuscript Author Manuscript Author Manuscript Author Manuscript

Though the most recent crystal 1.9 Å crystal structure by Shen et al. is believed to have considerably less damage to the OEC structure due to X-ray reduction, there still appear to be some structural differences, particularly when the Mn⋯Mn distances in this structure are compared to those measured by X-ray absorption fine structure (EXAFS) spectroscopy.[93,94] However, the broken-symmetry density functional theory (BS-DFT)-computed geometry of the OEC gives structural parameters that are consistent with the EXAFS results. Using these atomic coordinates and the calculated on-site expectation values for each Mn ion, we have constructed an analogous isosurface plot for putative methanol binding. These isosurface plots (SI Figures S7 and S8) are very similar to those generated using the Shen crystal structure coordinates and ^{55}Mn ENDOR derived projection factors (Figures 8 and 9) and also show exclusive overlap of the observed ^{13}C dipolar hyperfine isosurface plot with the methyl carbon position of methanol modeled at the W3 position.

According to the plots presented in Figure 8, methanol bound to calcium in place of W3 would be oriented such that the methyl group is rotated toward Mn4. This orientation is permitted by space-filling models based on the crystal structure coordinates which indicate no significant steric interactions with nearby amino acid residues. Interestingly, W3 is potentially involved in a hydrogen bonding network identified by Shen et al.[2] between the OEC and the redox active tyrosine Y_Z, which mediates electron transfer between the OEC and P_{680}^+. A single water (WY_Z) is positioned between Y_Z and W3, and likely forms hydrogen bonds to both. Methanol binding in place of W3 could still form a hydrogen bond with WY_Z, provided that the methyl group is oriented away from this water in a manner consistent with the isosurface plot in Figure 8. A structural model of this hydrogen bonding network identified in the 1.9 Å crystal structure linking the four water ligands of the OEC to Y_Z that involves three matrix waters is shown in Figure 10 below. In this model, W3 has been substituted with methanol in a position consistent with the measured ^{13}C dipolar HFI.

The possibility that methanol does not interact directly with the Mn_4CaO_5 cluster and is simply present in close proximity must be considered as well. In order to evaluate this scenario, the same isosurface plot from Figure 8 is compared to the nuclear coordinates of matrix waters evident in the 1.9 Å crystal structure–indeed we identify five matrix waters, denoted W5–W9, within 5 Å of the Mn_4CaO_5 cluster that methanol could displace and doing so give rise to the observed ^{13}C HFI (these waters correspond to waters 51731, 51739, 51743, 51779, and 52202 in the 1.9 Å crystal structure).[2] The surface of a sphere extending 1.4 Å from the oxygen atom of each of these matrix waters shows the possible positions of a methyl carbon of a water displacing-methanol (Figure 11). Each sphere has some intersection with the ^{13}C dipolar HFI isosurface plot.

Although any of these matrix waters are plausible candidates for methanol displacement, because of the effects that the presence of methanol has on the EPR signals of nearly all observed S states, and based on the linear response to the miss rate of S_i state turnover to methanol concentration, it is more likely that there is some direct interaction of methanol with the Mn_4CaO_5 cluster. Of these waters, only water 6 and 7 are likely to form hydrogen bonds directly to the cluster through μ-oxido bridges O4 and O1, respectively. These two waters are highlighted in Figure 12 below.

Author Manuscript Author Manuscript Author Manuscript Author Manuscript

Displacement of W6 by methanol could conceivably alter the hydrogen bond to O4 and slightly perturb the exchange pathway between Mn4 and the Mn_3O_4Ca cubane portion of the OEC. Methanol has been shown to form stronger hydrogen-bonds than water,[95,96] so it would be expected that there would be less effective protonation of the bridging oxygen. This could potentially lead to a small increase in the effective antiferromagnetic coupling between these two subunits of the Mn_4CaO_5 cluster, similar to the effect of deprotonation of μ-oxido bridges in exchange-coupled mixed-valence Mn compounds that greatly increases the exchange coupling between respective spin centers.[82] This may explain the observed increase in Δ for the S_2 state in the presence of MeOH, a detail discussed in more detail below. W7 also appears likely to participate in hydrogen bonding to the Mn_4CaO_5 cluster, in this case through the μ-oxido bridge O1. The effect of displacement of this water by methanol on the magnetic properties of the OEC is less straightforward to envision, though it could conceivably affect the exchange coupling between Mn1 and Mn2 in a manner analogous to that discussed for displacement of W6 by MeOH.

These two second coordination sphere waters are each part of two water access channels that lead to the OEC identified by computational analysis of X-ray crystal structures performed by Ho and co-workers.[38,97] Specifically, W6 appears to be near a branch point between two channels termed “narrow” and “broad” which would be accessible by methanol according to the study by Ho et al., whereas W7 appears to reside within the “back” channel which provides access to the Ca^{2+} ion, but does not contact the Mn ions of the Mn_4CaO_5 cluster.[38] Binding of methanol in place of either of these two waters could conceivably disrupt delivery of substrate waters to the cluster due to steric blocking of the water channel, regardless of the mechanism of water splitting. This blocking of the substrate access may explain the increase of the miss factor in the presence of methanol.

Electronic Structure Effects of Methanol Addition on the S_2 State

As was mentioned in the introduction, MeOH treatment has two primary effects on the magnetic properties of the S_2 state of the Mn_4CaO_5 cluster.

(1) The presence of MeOH (or other small, primary alcohols) shifts the equilibrium between the low-spin ($S = 1/2$) and high-spin ($S = 5/2$) conformations of S_2 strongly to the low-spin conformation. This equilibrium is also affected by the inclusion of a number of other chemical additives to the sample buffer, some favoring the low-spin conformation (50% glycerol, 30% polyethylene glycol) with others favoring the high-spin conformation (sucrose,[49,98] certain amines,[99] F^-,[100] and other inhibitors of Cl^- binding[101–103]). These two signals represent distinct ground states, as opposed to sublevels of the same electron spin manifold, and they can be interconverted by near-infrared illumination at cryogenic temperatures. Notably, the addition of methanol prevents this conversion by near-IR light. Recently, DFT calculations have predicted that these two interconvertable states arise from two nearly isoenergetic structural isomers of the Mn_4CaO_5 cluster which differ by the connectivity of the O5 μ-oxido bridge.[12] In this model, the low-spin ($S = 1/2$) MLS signal is produced by an “open cubane” form of the cluster, in which O5 is directly bound to Mn4, and not to Mn1, while the high-spin ($S = 5/2$) signal is produced by a “closed cubane” form in which O5 is bound to Mn1 and not Mn4.[12] The calculated difference in energy between

Author Manuscript Author Manuscript Author Manuscript Author Manuscript

these structures was only 1 kcal, which is likely the cause for the high degree of sensitivity of the equilibrium between the two forms to such a large number of seemingly disparate chemical additives. While the effect of methanol on this equilibrium has previously been attributed to some direct interaction with Mn ions of the OEC in the S_2 state, the findings of the present study appear to rule this out. Instead, it seems likely that small primary alcohols disrupt the hydrogen bonding network formed by the solvation shell about the OEC, leading to stabilization of the low-spin, open cubane form of the S_2 state.

(2) The presence of methanol also increases Δ, the energy separation between the lowest-energy spin manifold ($S = 1/2$) of the low-spin form of S_2 and the first, higher-energy manifold ($S = 3/2$).[19,32] As mentioned in the introduction, this increase in Δ reduces the anisotropy of the ^{55}Mn HFI tensors owing to a diminished relative contribution from the Mn(III) ZFS (we assume the magnitude of this ZFS is unaffected by MeOH addition).[32,69] Su and co-workers utilized a simplified spin-coupling model of the S_2 state in which the relative energies of the spin manifolds of the $S = 1/2$ ground state are proportional to a single effective coupling constant J_{eff} (with $\Delta = 3/2J_{eff}$), which represents the coupling between the monomeric "dangler" Mn4 ($S = 3/2$) and the $CaMn_3$ cluster (in either the $S = 1$ or 2 state).[32] Thus, the increase in Δ upon MeOH addition signals an increase in J_{eff}. Previously, this change in Δ was suggested to result from direct interaction/ligation of MeOH with at least one of the Mn ions of the OEC,[31–33,35,36] with the alcohol displacing one of the terminal waters on Mn4 or displacing the carboxyl group of Glu189 bound to Mn1 being favored.[31,32,47] These same two putative methanol-binding sites have also been proposed by Sjöholm et al, who suggest that Mn4 and Mn1 represent the high and low affinity binding sites for MeOH, respectively.[34] The findings of the present study disfavor both of these scenarios. Instead, we propose that that the effect of methanol on Δ stems from disruption of the hydrogen bonding network about the OEC due to its binding in place of W3 at the Ca^{2+} ion, or perturbation of the exchange pathways within the cluster due to displacement of waters which form hydrogen bonds to the μ-oxido bridges in the OEC. For the latter case, displacement of W6 by methanol is expected to affect the H-bonding to O4. ^{13}C-labeled methanol bound at either of these two sites could produce a ^{13}C dipolar HFI consistent with our present measurements.

While it is tempting to draw conclusions as to the identity of the substrate waters for O–O bond formation based on the revised evaluation of the potential binding sites for MeOH presented in the current study, in the context of the observed increase in the S_1-turnover miss rate α, there are several factors that prevent a definitive identification as of yet. First, the S_2 state is still two photo-oxidation events removed from the formation of the O–O bond and elimination of O_2, and the site-specific exchange rate between water and methanol is likely fast in comparison to the delay between flashes (0.5 s) that was used for the FIOPs measurements from which the MeOH dependence on the miss factor was determined. It is also uncertain whether the binding site of methanol is the same at each S-state, and the FIOPs method does not give any S-state specific information about inhibition of O_2 evolution. Even if MeOH binds in place of W3 at all S-states, it may be that the cause of the increase in the miss factor is simply the introduction of the methyl group between Y_z and the OEC, hindering oxidation of the Mn_4CaO_5 cluster by $Y_z^{\bullet}$, rather than acting specifically through competitive substrate inhibition. Because of these factors, no definitive statement

Author Manuscript Author Manuscript Author Manuscript Author Manuscript

can be made regarding the involvement of W3 in O–O bond formation from the current study, though it appears likely to be displaced by MeOH in the S_2 state. Further studies are required to evaluate the possibility of multiple binding sites for MeOH to the OEC in the S_2 state, as well as evaluation of the MeOH binding sites at more advanced S-states.

CONCLUSIONS

In conclusion, the multifrequency EPR and ENDOR spectroscopic analysis of methanol binding to Mn(III,IV)salpn and to PSII poised in the S_2 state presented here argue strongly that methanol does not bind directly to any Mn ion in the S_2 state of the Mn_4CaO_5 cluster in PSII. Instead, structural models of potential binding sites for methanol constrained by the observed ^{13}C dipolar HFI indicate that methanol likely binds in place of W3, a water ligand on Ca^{2+}, or in place of one of two waters identified in the 1.9 Å crystal structure that are likely to form hydrogen bonds to the Mn_4CaO_5 cluster through μ-oxido bridges O4 and O1, respectively. It is also possible that methanol binds at more than one of these sites, as all three could result in very similar effective ^{13}C dipolar HFI.

Supplementary Material

Refer to Web version on PubMed Central for supplementary material.

Acknowledgments

Funding

This work was funded by the Division of Chemical Sciences, Geosciences, and Biosciences (R.D.B. Award No. DE-FG02-11ER16282) of the Office of Basic Energy Sciences of the U.S. Department of Energy.

References

1. Larson E, Haddy A, Kirk ML, Sands RH, Hatfield WE, Pecoraro VL. The Asymmetric Mixed-Valent Complex (Mn(2-OH-3,5-Cl_2-SALPN)$_2$(THF))ClO_4 Shows A Temperature-Dependence Interconversion Between g=2 Multiline and Low-Field EPR Signals. J Am Chem Soc. 1992; 114:6263–6265.
2. Umena Y, Kawakami K, Shen JR, Kamiya N. Crystal structure of oxygen-evolving photosystem II at a resolution of 1.9 angstrom. Nature. 2011; 473:55–U65. [PubMed: 21499260]
3. Ferreira KN, Iverson TM, Maghlaoui K, Barber J, Iwata S. Architecture of the photosynthetic oxygen-evolving center. Science. 2004; 303:1831–1838. [PubMed: 14764885]
4. Loll B, Kern J, Saenger W, Zouni A, Biesiadka J. Towards complete cofactor arrangement in the 3.0 angstrom resolution structure of photosystem II. Nature. 2005; 438:1040–1044. [PubMed: 16355230]
5. McEvoy JP, Brudvig GW. Water-splitting chemistry of photosystem II. Chem Rev. 2006; 106:4455–4483. [PubMed: 17091926]
6. Kok B, Forbush B, McGloin M. Cooperation of Charges in Photosynthetic O_2 Evolution 1. A Linear 4-Step Mechanism. Photochem Photobiol. 1970; 11:457–475. [PubMed: 5456273]
7. Stich TA, Yeagle GJ, Service RJ, Debus RJ, Britt RD. Ligation of D1-His332 and D1-Asp170 to the Manganese Cluster of Photosystem II from Synechocystis Assessed by Multi-frequency Pulse EPR Spectroscopy. Biochemistry. 2011; 50:7390–7404. [PubMed: 21790179]
8. Cox N, Retegan M, Neese F, Pantazis DA, Boussac A, Lubitz W. Electronic structure of the oxygen-evolving complex in photosystem II prior to O-O bond formation. Science. 2014; 345:804–808. [PubMed: 25124437]

Author Manuscript Author Manuscript Author Manuscript Author Manuscript

9. Britt RD, Oyala PH. One step closer to O2. Science. 2014; 345:736. [PubMed: 25124415]
10. Peloquin JM, Campbell KA, Randall DW, Evanchik MA, Pecoraro VL, Armstrong WH, Britt RD. Mn-55 ENDOR of the S-2-state multiline EPR signal of photosystem II: Implications on the structure of the tetranuclear Mn cluster. J Am Chem Soc. 2000; 122:10926–10942.
11. Kulik LV, Epel B, Lubitz W, Messinger J. Electronic Structure of the Mn4OxCa Cluster in the S0 and S2 States of the Oxygen-Evolving Complex of Photosystem II Based on Pulse 55Mn-ENDOR and EPR Spectroscopy. J Am Chem Soc. 2007; 129:13421–13435. [PubMed: 17927172]
12. Pantazis DA, Ames W, Cox N, Lubitz W, Neese F. Two Interconvertible Structures that Explain the Spectroscopic Properties of the Oxygen-Evolving Complex of Photosystem II in the S2 State. Angew Chem, Int Ed. 2012; 51:9935–9940.
13. Beck WF, Depaula JC, Brudvig GW. Ammonia Binds to the Manganese site of The O2-Evolving Complex of Photosystem II in the S2 State. J Am Chem Soc. 1986; 108:4018–4022.
14. Andréasson LE, Hansson Ö, von Schenck K. The interaction of ammonia with the photosynthetic oxygen-evolving system. Biochim Biophys Acta. 1988; 936:351–360.
15. Britt RD, Zimmermann JL, Sauer K, Klein MP. Ammonia Binds to the Catalytic Mn of the Oxygen-Evolving Complex of Photosystem-II: Evidence by Electron-Spin Echo Envelope Modulation Spectroscopy. J Am Chem Soc. 1989; 111:3522–3532.
16. Boussac A, Rutherford AW, Styring S. Interaction of Ammonia With the Water Splitting Enzyme of Photosystem-II. Biochemistry. 1990; 29:24–32. [PubMed: 2157480]
17. Andréasson LE, Lindberg K. The inhibition of photosynthetic oxygen evolution by ammonia probed by EPR. Biochim Biophys Acta. 1992; 1100:177–183.
18. Dau H, Andrews JC, Roelofs TA, Latimer MJ, Liang WC, Yachandra VK, Sauer K, Klein MP. Structural Consequences of Ammonia Binding to The Manganese Center of the Photosynthetic Oxygen-Evolving Complex - an X-ray Absorption Spectroscopy Study of Isotropic and Oriented Photosystem-II Particles. Biochemistry. 1995; 34:5274–5287. [PubMed: 7711049]
19. Lorigan GA, Britt RD. Electron spin-lattice relaxation studies of different forms of the S2 state multiline EPR signal of the Photosystem II oxygen-evolving complex. Photosynth Res. 2000; 66:189–198. [PubMed: 16228419]
20. Chu HA, Feng YW, Wang CM, Chiang KA, Ke SC. Ammonia-induced structural changes of the oxygen-evolving complex in photosystem II as revealed by light-induced FTIR difference spectroscopy. Biochemistry. 2004; 43:10877–10885. [PubMed: 15323548]
21. Fang CH, Chiang KA, Hung CH, Chang KJ, Ke SC, Chu HA. Effects of ethylene glycol and methanol on ammonia-induced structural changes of the oxygen-evolving complex in photosystem II. Biochemistry. 2005; 44:9758–9765. [PubMed: 16008360]
22. Evans MCW, Ball RJ, Nugent JHA. Ammonia displaces methanol bound to the water oxidizing complex of photosystem II in the S-2 state. FEBS Lett. 2005; 579:3081–3084. [PubMed: 15896788]
23. Hou LH, Wu CM, Huang HH, Chu HA. Effects of Ammonia on the Structure of the Oxygen-Evolving Complex in Photosystem II As Revealed by Light-Induced FTIR Difference Spectroscopy. Biochemistry. 2011; 50:9248–9254. [PubMed: 21942297]
24. Navarro MP, Ames WM, Nilsson H, Lohmiller T, Pantazis DA, Rapatskiy L, Nowaczyk MM, Neese F, Boussac A, Messinger J, Lubitz W, Cox N. Ammonia binding to the oxygen-evolving complex of photosystem II identifies the solvent-exchangeable oxygen bridge (mu-oxo) of the manganese tetramer. Proc Natl Acad Sci U S A. 2013; 110:15561–15566. [PubMed: 24023065]
25. Messinger J, Renger G. The Reactivity of Hydrazine with Photosystem-II Strongly Depends on the Redox State of the Water Oxidizing System. FEBS Lett. 1990; 277:141–146. [PubMed: 2269344]
26. Kebekus U, Messinger J, Renger G. Structural-Changes in the Water-Oxidizing Complex Monitored via the PH-Dependence of the Reduction Rate of Redox State S-1 by Hydrazine and Hydroxylamine in Isolated Spinach Thylakoids. Biochemistry. 1995; 34:6175–6182. [PubMed: 7742322]
27. Fine PL, Frasch WD. The Oxygen-Evolving Complex Requires Chloride to Prevent Hydrogen-Peroxide Formation. Biochemistry. 1992; 31:12204–12210. [PubMed: 1457417]

Author Manuscript Author Manuscript Author Manuscript Author Manuscript

28. Song YG, Liu B, Wang LF, Li MH, Liu Y. Damage to the oxygen-evolving complex by superoxide anion, hydrogen peroxide, and hydroxyl radical in photoinhibition of photosystem II. Photosynth Res. 2006; 90:67–78. [PubMed: 17131094]
29. Haumann M, Bogershausen O, Cherepanov D, Ahlbrink R, Junge W. Photosynthetic oxygen evolution: H/D isotope effects and the coupling between electron and proton transfer during the redox reactions at the oxidizing side of Photosystem II. Photosynth Res. 1997; 51:193–208.
30. Randall DW, Gelasco A, Caudle MT, Pecoraro VL, Britt RD. ESE-ENDOR and ESEEM Characterization of Water and Methanol Ligation to a Dinuclear Mn(III)Mn(IV) Complex†. J Am Chem Soc. 1997; 119:4481–4491.
31. Force DA, Randall DW, Lorigan GA, Clemens KL, Britt RD. ESEEM studies of alcohol binding to the manganese cluster of the oxygen evolving complex of Photosystem II. J Am Chem Soc. 1998; 120:13321–13333.
32. Su JH, Cox N, Ames W, Pantazis DA, Rapatskiy L, Lohmiller T, Kulik LV, Dorlet P, Rutherford AW, Neese F, Boussac A, Lubitz W, Messinger J. The electronic structures of the S-2 states of the oxygen-evolving complexes of photosystem II in plants and cyanobacteria in the presence and absence of methanol. Biochim Biophys Acta. 2011; 1807:829–840. [PubMed: 21406177]
33. Åhrling KA, Evans MCW, Nugent JHA, Pace RJ. The two forms of the S2 state multiline signal in Photosystem II: effect of methanol and ethanol. Biochim Biophys Acta. 2004; 1656:66–77. [PubMed: 15136160]
34. Sjoholm J, Chen GY, Ho F, Mamedov F, Styring S. Split Electron Paramagnetic Resonance Signal Induction in Photosystem II Suggests Two Binding Sites in the S-2 State for the Substrate Analogue Methanol. Biochemistry. 2013; 52:3669–3677. [PubMed: 23621812]
35. Su JH, Havelius KGV, Mamedov F, Ho FM, Styring S. Split EPR signals from photosystem II are modified by methanol, reflecting S state-dependent binding and alterations in the magnetic coupling in the CaMn4 cluster. Biochemistry. 2006; 45:7617–7627. [PubMed: 16768457]
36. Deak Z, Peterson S, Geijer P, Ahrling KA, Styring S. Methanol modification of the electron paramagnetic resonance signals from the S-0 and S-2 states of the water-oxidizing complex of Photosystem II. Biochim Biophys Acta. 1999; 1412:240–249. [PubMed: 10482786]
37. Nöring B, Shevela D, Renger G, Messinger J. Effects of methanol on the S i -state transitions in photosynthetic water-splitting. Photosyn Res. 2008; 98:251–260. [PubMed: 18819015]
38. Ho FM, Styring S. Access channels and methanol binding site to the CaMn4 cluster in Photosystem II based on solvent accessibility simulations, with implications for substrate water access. Biochim Biophys Acta. 2008; 1777:140–153. [PubMed: 17964532]
39. Lohmiller T, Cox N, Su JH, Messinger J, Lubitz W. The Basic Properties of the Electronic Structure of the Oxygen-evolving Complex of Photosystem II Are Not Perturbed by Ca2+ Removal. J Biol Chem. 2012; 287:24721–24733. [PubMed: 22549771]
40. Fang CH, Chiang KA, Hung CH, Chang K, Ke SC, Chu HA. Effects of Ethylene Glycol and Methanol on Ammonia-Induced Structural Changes of the Oxygen-Evolving Complex in Photosystem II. Biochemistry. 2005; 44:9758–9765. [PubMed: 16008360]
41. Miller AF, Brudvig GW. A Guide to Electron-Paramagnetic Resonance Spectroscopy of Photosystem-II Membranes. Biochim Biophys Acta. 1991; 1056:1–18. [PubMed: 1845842]
42. Messinger J, Nugent JHA, Evans MCW. Detection of an EPR multiline signal for the S-0 state in photosystem II. Biochemistry. 1997; 36:11055–11060. [PubMed: 9333322]
43. Kulik LV, Epel B, Lubitz W, Messinger J. Mn-55 pulse ENDOR at 34 GHz of the S-0 and S-2 states of the oxygen-evolving complex in photosystem II. J Am Chem Soc. 2005; 127:2392–2393. [PubMed: 15724984]
44. Ahrling KA, Peterson S, Styring S. The S-0 state EPR signal from the Mn cluster in photosystem II arises from an isolated S=1/2 ground state. Biochemistry. 1998; 37:8115–8120. [PubMed: 9609706]
45. Peterson S, Ahrling KA, Styring S. The EPR signals from the S-0 and S-2 states of the Mn cluster in photosystem II relax differently. Biochemistry. 1999; 38:15223–15230. [PubMed: 10563805]
46. Geijer P, Peterson S, Ahrling KA, Deak Z, Styring S. Comparative studies of the S-0 and S-2 multiline electron paramagnetic resonance signals from the manganese cluster in Photosystem II. Biochim Biophys Acta. 2001; 1503:83–95. [PubMed: 11115626]

Author Manuscript Author Manuscript Author Manuscript Author Manuscript

47. Åhrling KA, Evans MCW, Nugent JHA, Ball RJ, Pace RJ. ESEEM Studies of Substrate Water and Small Alcohol Binding to the Oxygen-Evolving Complex of Photosystem II during Functional Turnover†. Biochemistry. 2006; 45:7069–7082. [PubMed: 16752897]
48. Peloquin JM, Britt RD. EPR/ENDOR characterization of the physical and electronic structure of the OEC Mn cluster. Biochim Biophys Acta. 2001; 1503:96–111. [PubMed: 11115627]
49. Zimmermann JL, Rutherford AW. Electron-Paramagnetic Resonance Properties of the S-2 State of the Oxygen-Evolving Complex of Photosystem-II. Biochemistry. 1986; 25:4609–4615.
50. Dexheimer SL, Klein MP. Detection of a Paramagnetic Intermediate in the S1-State of the Photosynthetic Oxygen-Evolving Complex. J Am Chem Soc. 1992; 114:2821–2826.
51. Yamauchi T, Mino H, Matsukawa T, Kawamori A, Ono T. Parallel polarization electron paramagnetic resonance studies of the S-1-state manganese cluster in the photosynthetic oxygen-evolving system. Biochemistry. 1997; 36:7520–7526. [PubMed: 9200702]
52. Hsieh WY, Campbell KA, Gregor W, Britt RD, Yoder DW, Penner-Hahn JE, Pecoraro VL. The first spectroscopic model for the S-1 state multiline signal of the OEC. Biochim Biophys Acta. 2004; 1655:149–157. [PubMed: 15100027]
53. Haddy A, Lakshmi KV, Brudvig GW, Frank HA. Q-band EPR of the S-2 state of Photosystem II confirms an S=5/2 origin of the X-band g=4.1 signal. Biophys J. 2004; 87:2885–2896. [PubMed: 15454478]
54. Boussac A, Girerd JJ, Rutherford AW. Conversion of the spin state of the manganese complex in photosystem II induced by near-infrared light. Biochemistry. 1996; 35:6984–6989. [PubMed: 8679522]
55. Boussac A, Kuhl H, Un S, Rogner M, Rutherford AW. Effect of near-infrared light on the S-2-state of the manganese complex of photosystem II from Synechococcus elongatus. Biochemistry. 1998; 37:8995–9000. [PubMed: 9636042]
56. Boussac A, Un S, Horner O, Rutherford AW. High-spin states (S ≥ 5/2) of the photosystem II manganese complex. Biochemistry. 1998; 37:4001–4007. [PubMed: 9565450]
57. Kim DH, Britt RD, Klein MP, Sauer K. The g = 4.1 EPR Signal of the S2 State of the Photosynthetic Oxygen-Evolving Complex Arises from a Multinuclear Mn Cluster. J Am Chem Soc. 1990; 112:9389–9391.
58. Yano J, Pushkar Y, Glatzel P, Lewis A, Sauer K, Messinger J, Bergmann U, Yachandra V. High-resolution Mn EXAFS of the oxygen-evolving complex in photosystem II: Structural implications for the Mn4Ca cluster. J Am Chem Soc. 2005; 127:14974–14975. [PubMed: 16248606]
59. Berthold DA, Babcock GT, Yocum CF. A Highly Resolved, Oxygen-Evolving Photosystem-II Preparation From Spinach Thylakoid Membranes - Electron Paramagnetic Resonance and Electron Transport Properties. FEBS Lett. 1981; 134:231–234.
60. Ford RC, Evans MCW. Isolation of a photosystem 2 preparation from higher plants with highly enriched oxygen evolution activity. FEBS Lett. 1983; 160:159–164.
61. Stich TA, Lahiri S, Yeagle G, Dicus M, Brynda M, Gunn A, Aznar C, DeRose VJ, Britt RD. Multifrequency pulsed EPR studies of biologically relevant manganese(II) complexes. Appl Magn Reson. 2007; 31:321–341. [PubMed: 22190766]
62. Flores M, Isaacson RA, Calvo R, Feher G, Lubitz W. Probing hydrogen bonding to quinone anion radicals by 1H and 2H ENDOR spectroscopy at 35 GHz. Chem Phys. 2003; 294:401–413.
63. Stoll S, Schweiger A. EasySpin, a comprehensive software package for spectral simulation and analysis in EPR. J Magn Reson. 2006; 178:42–55. [PubMed: 16188474]
64. Stoll S, Britt RD. General and efficient simulation of pulse EPR spectra. Phys Chem Chem Phys. 2009; 11:6614–6625. [PubMed: 19639136]
65. Gemperle C, Schweiger A. Pulsed electron-nuclear double resonance methodology. Chem Rev. 1991; 91:1481–1505.
66. Sauer K, Yano J, Yachandra VK. X-ray spectroscopy of the Mn4Ca cluster in the water-oxidation complex of Photosystem II. Photosyn Res. 2005; 85:73–86. [PubMed: 15977060]
67. Pushkar Y, Yano J, Glatzel P, Messinger J, Lewis A, Sauer K, Bergmann U, Yachandra V. Structure and orientation of the Mn4Ca cluster in plant photosystem II membranes studied by polarized range-extended X-ray absorption spectroscopy. J Biol Chem. 2007; 282:7198–7208. [PubMed: 17190828]

Author Manuscript Author Manuscript Author Manuscript Author Manuscript

68. Zheng M, Khangulov SV, Dismukes GC, Barynin VV. Electronic structure of dimanganese(II,III) and dimanganese(III,IV) complexes and dimanganese catalase enzyme: a general EPR spectral simulation approach. Inorg Chem. 1994; 33:382–387.
69. Cox N, Rapatskiy L, Su JH, Pantazis DA, Sugiura M, Kulik L, Dorlet P, Rutherford AW, Neese F, Boussac A, Lubitz W, Messinger J. Effect of Ca^{2+}/Sr^{2+} Substitution on the Electronic Structure of the Oxygen-Evolving Complex of Photosystem II: A Combined Multifrequency EPR, Mn-55-ENDOR, and DFT Study of the S-2 State. J Am Chem Soc. 2011; 133:3635–3648. [PubMed: 21341708]
70. Hyde JS, Pasenkiewicz-Gierula M, Jesmanowicz A, Antholine WE. Pseudo field modulation in EPR spectroscopy. Appl Magn Reson. 1990; 1:483–496.
71. Cooper SR, Dismukes GC, Klein MP, Calvin M. EPR and Magnetic-Susceptibility Studies of Mixed-Valence Manganese Complexes. Abstr Papers Am Chem Soc. 1978; 175:216–216.
72. Haddy A, Waldo GS, Sands RH, Pennerhahn JE. Simulation of Multifrequency EPR-Spectra From Mn(III)/Mn(IV) Catalase of Lactobacillus-Plantarium using a New Approach Based on Perturbation-Theory. Inorg Chem. 1994; 33:2677–2682.
73. Zheng M, Dismukes GC. Orbital configuration of the valence electrons, ligand field symmetry, and manganese oxidation states of the photosynthetic water oxidizing complex: Analysis of the S-2 state multiline EPR signals. Inorg Chem. 1996; 35:3307–3319. [PubMed: 11666533]
74. Schweiger, A., Jeschke, G. Principles of Pulse Electron Paramagnetic Resonance. Oxford University Press; New York: 2001.
75. Fiege R, Zweygart W, Bittl R, Adir N, Renger G, Lubitz W. EPR and ENDOR studies of the water oxidizing complex of Photosystem II. Photosyn Res. 1996; 48:227–237. [PubMed: 24271303]
76. Cox N, Rapatskiy L, Su JH, Pantazis DA, Sugiura M, Kulik L, Dorlet P, Rutherford AW, Neese F, Boussac A, Lubitz W, Messinger J. SI - Effect of Ca^{2+}/Sr^{2+} Substitution on the Electronic Structure of the Oxygen-Evolving Complex of Photosystem II: A Combined Multifrequency EPR, 55Mn-ENDOR, and DFT Study of the S2 State. J Am Chem Soc. 2011; 133:3635–3648. [PubMed: 21341708]
77. Zhou YX, Zheng XF, Han D, Zhang HY, Shen XQ, Niu CY, Chen PK, Hou HW, Zhu Y. Syntheses and Crystal Structures of Fe(III) and Mn(III) Complexes with Salen Ligands: [Fe(salen)CL] ·CH3CN and [Mn(salen)(SCN)(CH_3OH)]·CH3CN. Synth React Inorg, Met-Org, Nano-Met Chem. 2006; 36:693–699.
78. Kessissoglou DP, Butler WM, Pecoraro VL. Characterization of mono- and binuclear manganese(II) Schiff base complexes with metal-disulfide ligation. Inorg Chem. 1987; 26:495–503.
79. Lohmiller T, Krewald V, Navarro MP, Retegan M, Rapatskiy L, Nowaczyk MM, Boussac A, Neese F, Lubitz W, Pantazis DA, Cox N. Structure, ligands and substrate coordination of the oxygen-evolving complex of photosystem II in the S2 state: a combined EPR and DFT study. Phys Chem Chem Phys. 2014; 16:11877–11892. [PubMed: 24525937]
80. Rapatskiy L, Cox N, Savitsky A, Ames WM, Sander J, Nowaczyk MM, Roegner M, Boussac A, Neese F, Messinger J, Lubitz W. Detection of the Water-Binding Sites of the Oxygen-Evolving Complex of Photosystem II Using W-Band O-17 Electron-Electron Double Resonance-Detected NMR Spectroscopy. J Am Chem Soc. 2012; 134:16619–16634. [PubMed: 22937979]
81. Siegbahn PEM. Water oxidation mechanism in photosystem II, including oxidations, proton release pathways, O-O bond formation and O-2 release. Biochim Biophys Acta. 2013; 1827:1003–1019. [PubMed: 23103385]
82. Baldwin MJ, Stemmler TL, Riggsgelasco PJ, Kirk ML, Pennerhahn JE, Pecoraro VL. Structural and Magnetic Effects of Successive Protonation of Oxo-Bridges in High-Valent Manganese Dimers. J Am Chem Soc. 1994; 116:11349–11356.
83. Pantazis DA, Krewald V, Orio M, Neese F. Theoretical magnetochemistry of dinuclear manganese complexes: broken symmetry density functional theory investigation on the influence of bridging motifs on structure and magnetism. Dalton Trans. 2010; 39:4959–4967. [PubMed: 20419188]
84. Yeagle GJ, Gilchrist ML, McCarrick RM, Britt RD. Multifrequency pulsed electron paramagnetic resonance study of the S-2 state of the photosystem II manganese cluster. Inorg Chem. 2008; 47:1803–1814. [PubMed: 18330971]

Author Manuscript Author Manuscript Author Manuscript Author Manuscript

85. Stich TA, Whittaker JW, Britt RD. Multifrequency EPR Studies of Manganese Catalases Provide a Complete Description of Protemaceous Nitrogen Coordination. J Phys Chem B. 2010; 114:14178–14188. [PubMed: 20055466]

86. Chen H, Faller JW, Crabtree RH, Brudvig GW. Dimer-of-Dimers Model for the Oxygen-Evolving Complex of Photosystem II. Synthesis and Properties of [MnIV4O5(terpy)4-(H2O)2](ClO4)6. J Am Chem Soc. 2004; 126:7345–7349. [PubMed: 15186173]

87. Chen, Collomb M-N, Duboc C, Blondin G, Rivière E, Faller JW, Crabtree RH, Brudvig GW. New Linear High-Valent Tetranuclear Manganese-Oxo Cluster Relevant to the Oxygen-Evolving Complex of Photosystem II with Oxo, Hydroxo, and Aqua Coordinated to a Single Mn(IV). Inorg Chem. 2005; 44:9567–9573. [PubMed: 16323946]

88. Yamazaki H, Igarashi S, Nagata T, Yagi M. Substituent Effects on Core Structures and Heterogeneous Catalytic Activities of MnIII(μ-O)2MnIV Dimers with 2,2′:6′,2″-Terpyridine Derivative Ligands for Water Oxidation. Inorg Chem. 2012; 51:1530–1539. [PubMed: 22280017]

89. Pellissier A, Bretonnière Y, Chatterton N, Pécaut J, Delangle P, Mazzanti M. Relating Structural and Thermodynamic Effects of the Pb(II) Lone Pair: A New Picolinate Ligand Designed to Accommodate the Pb(II) Lone Pair Leads to High Stability and Selectivity. Inorg Chem. 2007; 46:3714–3725. [PubMed: 17411031]

90. Kalibabchuk VA, Usenko NI, Golenya IA, Iskenderov TS, Haukka M. Poly[bis[[mu]4-*N*-(2-hydroxyiminopro-pionyl)-*N*′-(2-oxidoiminopropionyl)propane-1,3-diaminato]-dimethanolcalciumdicopper(II)]. Acta Crystallogr, Sect E. 2009; 65:m1139–m1140.

91. Owczarek E, Hawlicka E. Molecular dynamics study of $CaCl_2$ in methanol. J Phys Chem B. 2006; 110:22712–22718. [PubMed: 17092020]

92. Owczarek E, Rybicki M, Hawlicka E. Solvation of calcium ions in methanol-water mixtures: Molecular dynamics simulation. J Phys Chem B. 2007; 111:14271–14278. [PubMed: 18062680]

93. Yano J, Kern J, Irrgang KD, Latimer MJ, Bergmann U, Glatzel P, Pushkar Y, Biesiadka J, Loll B, Sauer K, Messinger J, Zouni A, Yachandra VK. X-ray damage to the Mn4Ca complex in single crystals of photosystem II: A case study for metalloprotein crystallography. Proc Natl Acad Sci U S A. 2005; 102:12047–12052. [PubMed: 16103362]

94. Pushkar YL, Yano J, Sauer K, Boussac A, Yachandra VK. Structural changes in the Mn4Ca cluster and the mechanism of photosynthetic water splitting. Proc Natl Acad Sci U S A. 2008; 105:1879–1884. [PubMed: 18250316]

95. Fileti EE, Chaudhuri P, Canuto S. Relative strength of hydrogen bond interaction in alcohol–water complexes. Chem Phys Lett. 2004; 400:494–499.

96. Sasaki H, Daicho S, Yamada Y, Nibu Y. Comparable Strength of OH–O versus OH–π Hydrogen Bonds in Hydrogen-Bonded 2,3-Benzofuran Clusters with Water and Methanol. J Phys Chem A. 2013; 117:3183–3189. [PubMed: 23517236]

97. Linke K, Ho FM. Water in Photosystem II: Structural, functional and mechanistic considerations. Biochim Biophys Acta. 2014; 1837:14–32. [PubMed: 23978393]

98. Zimmermann JL, Rutherford AW. Electron-Paramagnetic-Resonance Studies of the Oxygen-Evolving Enzyme of Photosystem-II. Biochim Biophys Acta. 1984; 767:160–167.

99. Beck WF, Brudvig GW. Effects of Amine Binding on the Manganese Site of the Oxygen-Evolving Complex of Photosystem-II. Biophys J. 1986; 49:A485–A485.

100. DeRose VJ, Latimer MJ, Zimmermann JL, Mukerji I, Yachandra VK, Sauer K, Klein MP. Fluoride substitution in the Mn cluster from Photosystem II: EPR and X-ray absorption spectroscopy studies. Chem Phys. 1995; 194:443–459.

101. Debus RJ. The Manganese and Calcium-Ions of Photosynthetic Oxygen Evolution. Biochim Biophys Acta. 1992; 1102:269–352. [PubMed: 1390827]

102. Haddy A, Dunham WR, Sands RH, Aasa R. Multifrequency EPR Investigations into the Origin of the S2-state Signal at $g = 4$ of the O_2-Evolving Complex. Biochim Biophys Acta. 1992; 1099:25–34. [PubMed: 1310873]

103. Vanvliet P, Boussac A, Rutherford AW. Chloride-Depletion Effects in the Calcium-Deficient Oxygen-Evolving Complex of Photosystem-II. Biochemistry. 1994; 33:12998–13004. [PubMed: 7947704]

Author Manuscript Author Manuscript Author Manuscript Author Manuscript

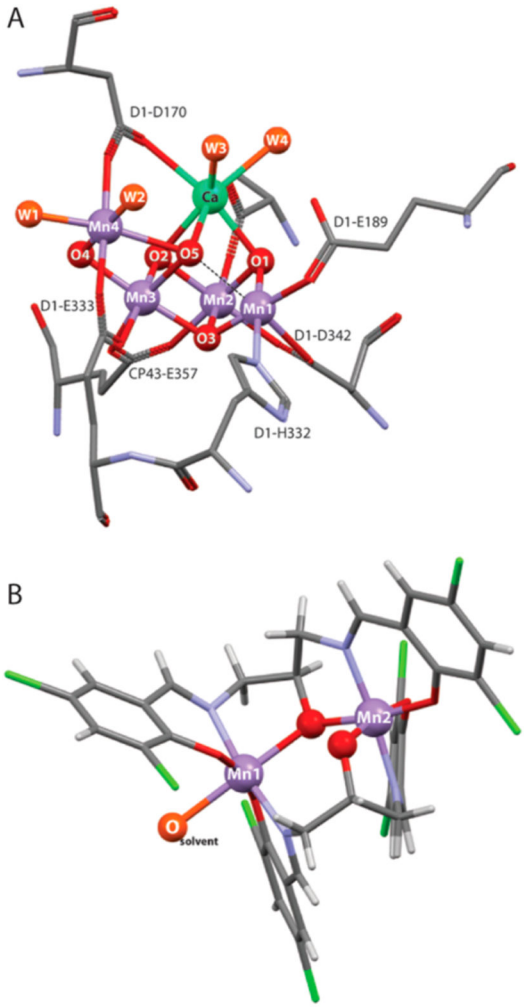

Figure 1.

(A) A structure of the OEC and selected ligands from the 1.9 Å crystal structure (PDB 3ARC).[2] The dotted line indicates a possibly labile bond between O5 and Mn1.[12] Oxygen atoms of ligand waters W(1–4) are shown in orange. (B) A structure of (2-OH-3,5-Cl_2-salpn)$_2$Mn(III)Mn(IV) + solvent. Oxidation states of Mn ions in the salpn complex are Mn1 = Mn(III), Mn2 = Mn(IV). The oxygen atom of the solvent ligand is shown in orange. The atomic coordinates used are from the crystal structure of Mn(III,IV)salpn + tetrahydrofuran (THF).[1]

Author Manuscript Author Manuscript Author Manuscript Author Manuscript

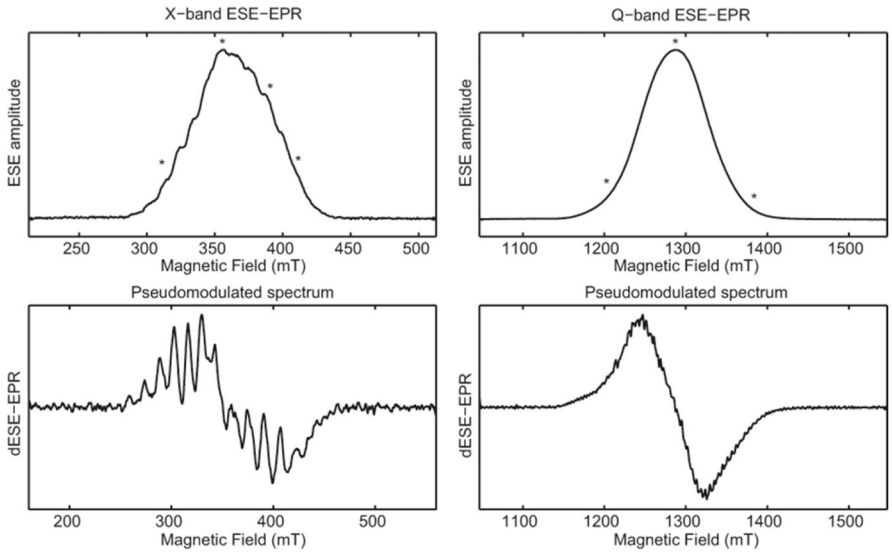

Figure 2.

X-band (left) and Q-band (right) ESE-detected EPR spectra of Mn(III,IV)salpn + ^{13}C methanol. Bottom panels represent the pseudomodulated (2 mT) spectrum of each respective ESE-EPR spectrum. Acquisition parameters: X-band: temperature = 4.5 K; ν_{MW} = 9.742 GHz; $\pi/2_{MW}$ = 100 ns; tau = 400 ns; srt = 6 μs. Q-band: temperature = 4.5 K; ν_{MW} = 34.079 GHz; $\pi/2_{MW}$ = 120 ns; tau = 500 ns; shot repetition time (srt) = 6 ms. Asterisks indicate field positions at which X-band HYSCORE (see Figure 3) and Q-band Mims ENDOR (see Figure 4) were acquired.

Author Manuscript Author Manuscript Author Manuscript Author Manuscript

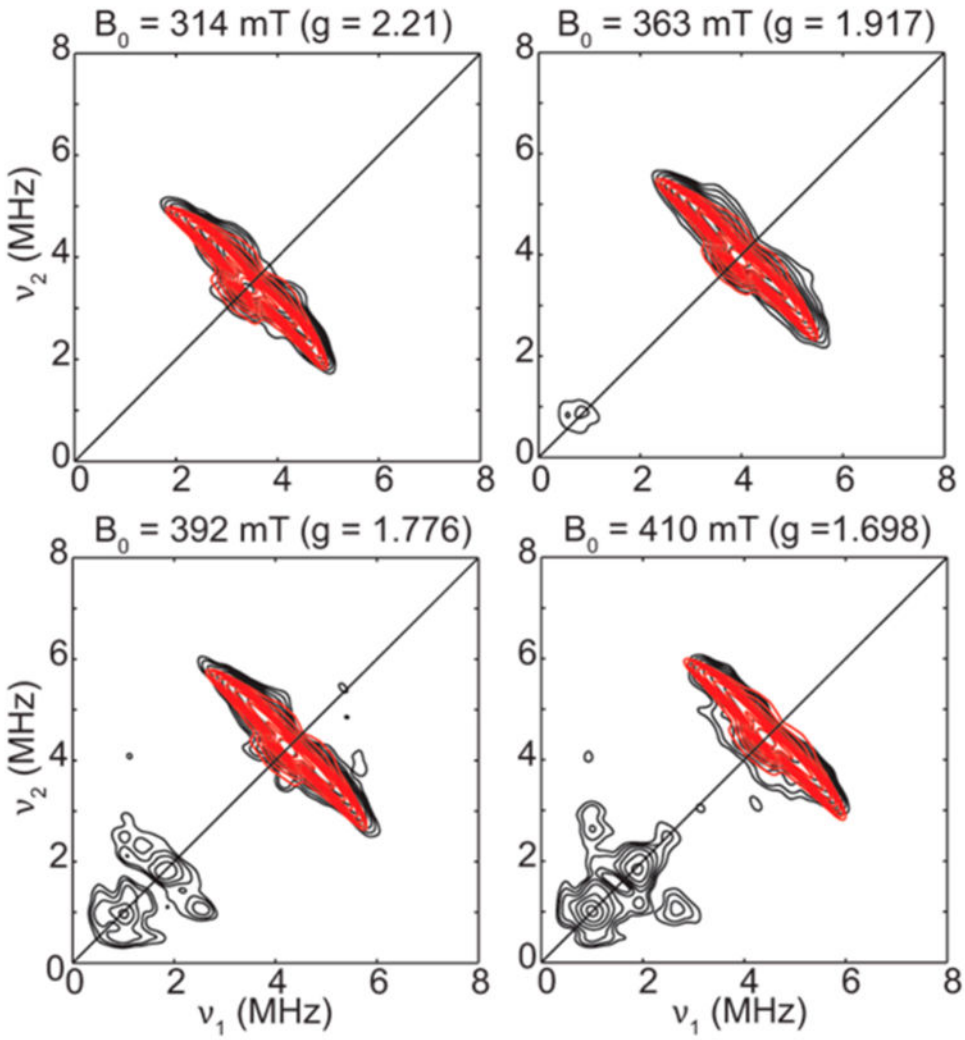

Figure 3.

X-band HYSCORE of Mn(III,IV)salpn + ^{13}C methanol at four different field positions. Black contours represent the 2D Fourier transform of the experimental data, red contours represent the spectral simulation of signals from ^{13}C using the parameters in Table 1. Acquisition parameters: temperature = 4.5 K; ν_{MW} = 9.742 GHz; $\pi/2_{MW}$ = π_{MW} = 16 ns; tau = 148 ns (314 mT) 128 ns (363 and 392 mT) and 120 ns (410 mT); T_1 = T_2 = 100 ns; ΔT_1 = ΔT_2 = 20 ns; srt = 6ms.

Author Manuscript Author Manuscript Author Manuscript Author Manuscript

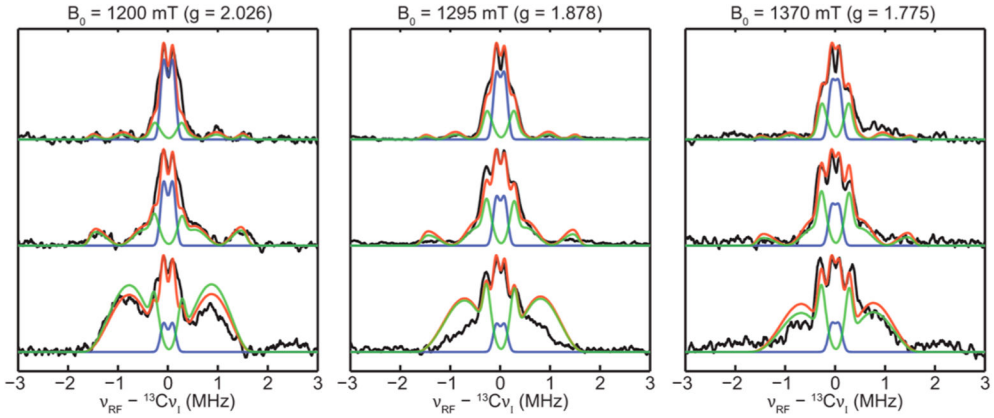

Figure 4.

Q-band ^{13}C Mims ENDOR spectra of Mn(III,IV)salpn + ^{13}C methanol: Traces in black represent spectra collected at three tau values—800, 500, and 300 ns—from top to bottom, respectively. Colored traces represent two component simulations at each tau and field position: weakly coupled "matrix" ^{13}C in blue, strongly coupled ^{13}C in green, and the combined simulation in red. Experimental data have been smoothed using a three-point Savitsky–Golay filter. Weighting of the two simulation components are 1:10 strongly/weakly coupled ^{13}C species. Acquisition parameters: temperature = 4.5 K; ν_{MW} = 34.038 GHz; $\pi/2_{MW}$ = 12 ns; π_{RF} = 20 μs; srt = 6 ms. Simulation parameters are the same as those used in Figure 3, and they are listed in Table 1.

Author Manuscript Author Manuscript Author Manuscript Author Manuscript

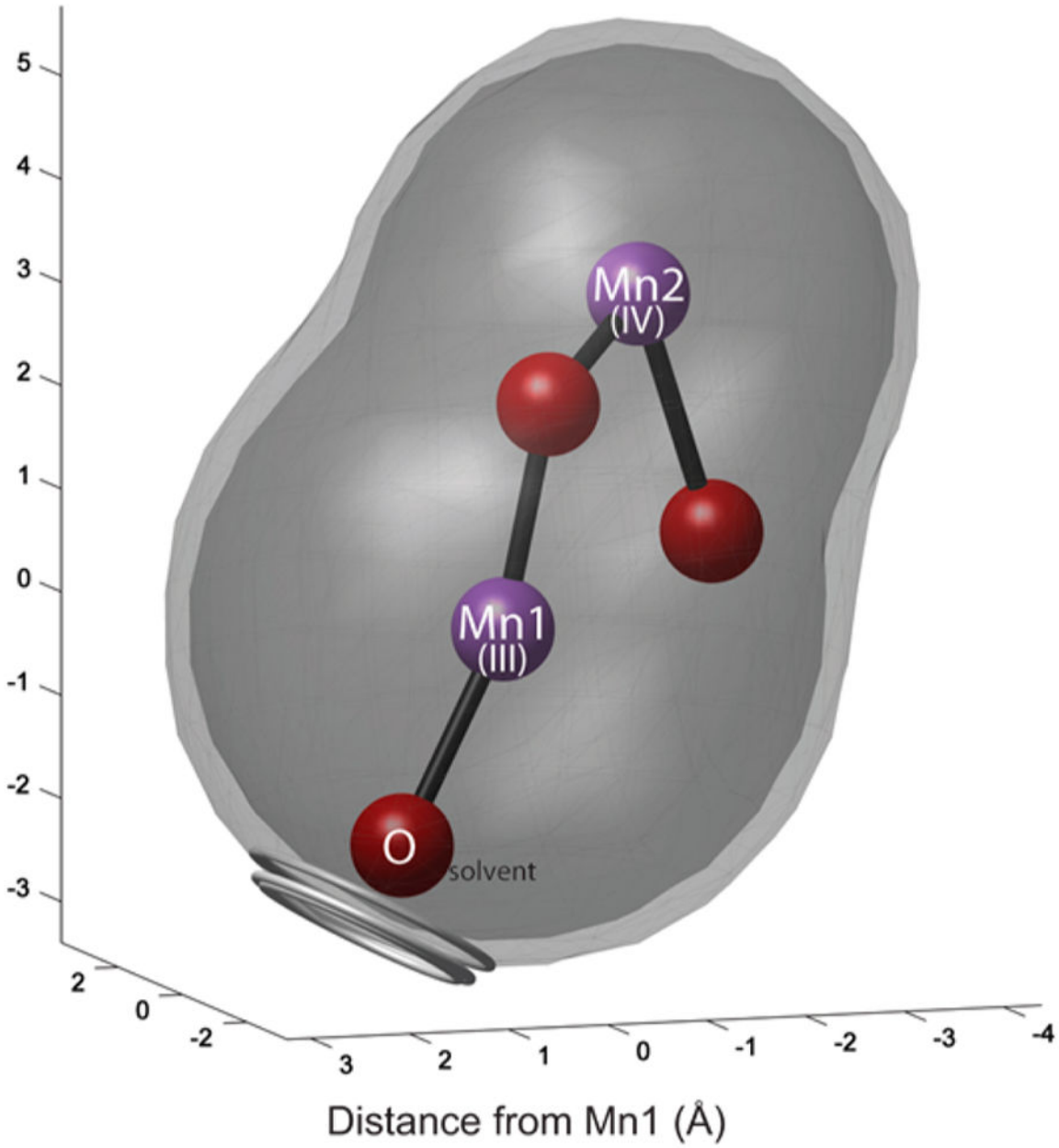

Figure 5.

^{13}C Dipolar isosurface plot representing possible position of the methyl ^{13}C nucleus magnetically coupled to Mn(III,IV)salpn + methanol. Inner and outer dark gray surfaces were calculated using the upper and lower limits of isotropic spin projections calculated using previously published ^{55}Mn A_{iso} values for Mn(III,IV)salpn + THF, the range of intrinsic ^{55}Mn HFI reported for mononuclear Mn(III) and Mn(IV) compounds (see Table 2) and measured ^{13}C dipolar HFI (see Table 1). Light gray rings are radial distributions of probable locations of the methyl carbon of methanol bound to the Mn(III) calculated using bond angles and distances from published crystal structures of synthetic molecules with

methanol bound directly to manganese with the longest,[77] average, and shortest[78] metal–carbon distances from Mn.

Author Manuscript Author Manuscript Author Manuscript Author Manuscript

Author Manuscript Author Manuscript Author Manuscript Author Manuscript

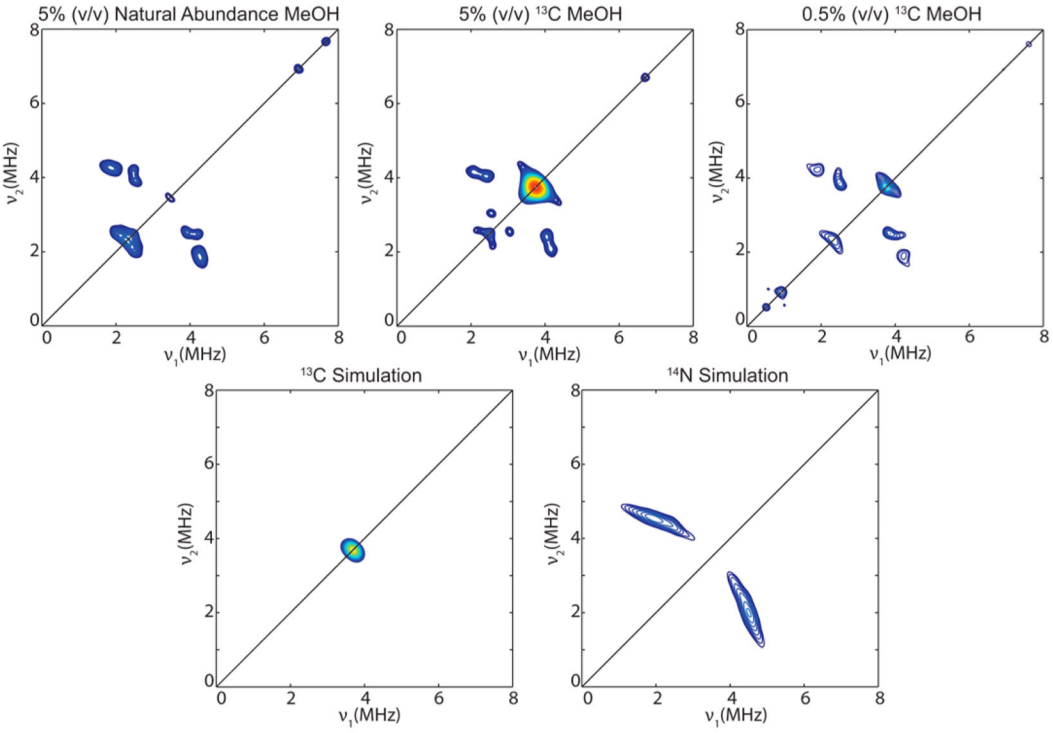

Figure 6.

X-band HYSCORE spectra of the S_2 state of PSII. Top panels from left to right: PSII + 5% (v/v) natural abundance methanol, 5% (v/v) ^{13}C methanol and 0.5% (v/v) ^{13}C methanol, respectively. Bottom panels represent the spectral simulations of signals from the ^{13}C nucleus of methanol (see Table 1) and the ^{14}N nucleus of His332. Acquisition parameters: Temperature = 4.5 K; ν_{MW} = 9.489 GHz (^{13}C), ν_{MW} = 9.472 GHz (nat. abund.); B_0 = 348 mT (g = 1.98); $\pi/2_{MW} = \pi_{MW}$ = 24 ns; tau = 136 ns; $T_1 = T_2$ = 100 ns; $\Delta T_1 = \Delta T_2$ = 20 ns; srt =5 ms.

Author Manuscript Author Manuscript Author Manuscript Author Manuscript

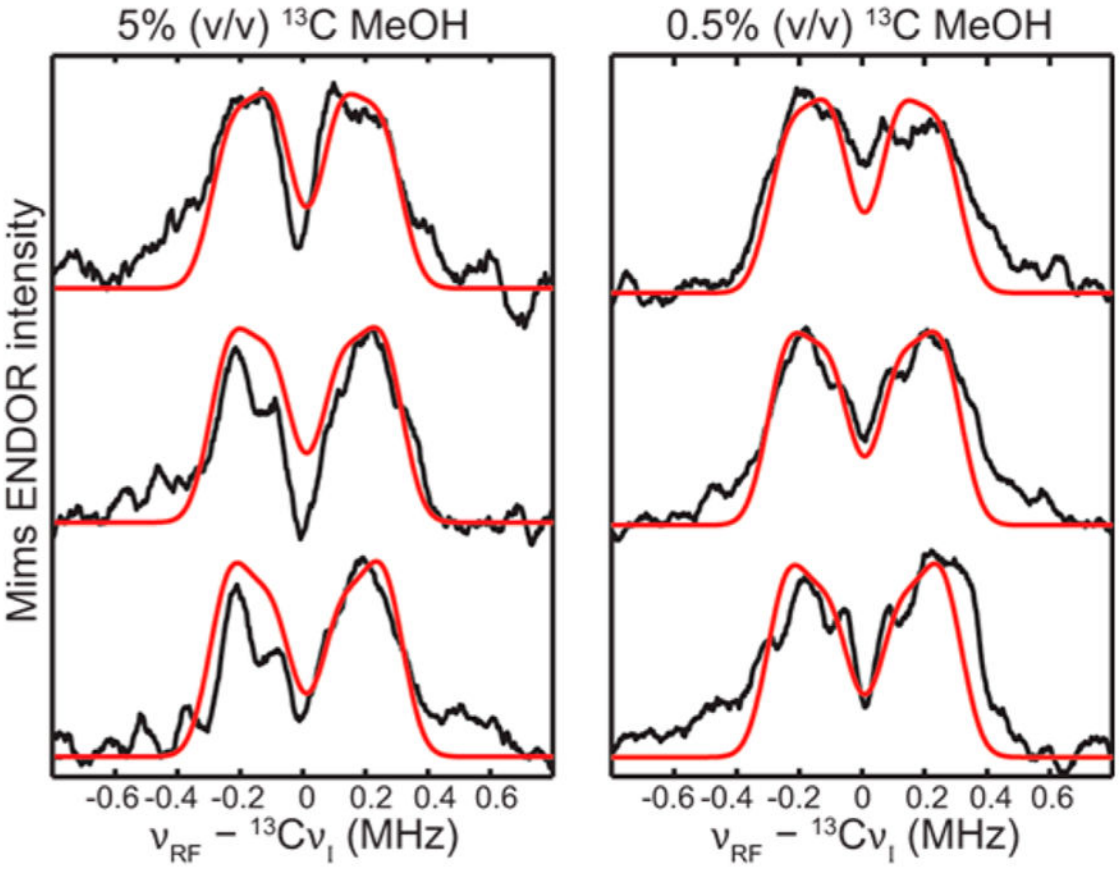

Figure 7.

Light-minus-dark Q-band ^{13}C Mims ENDOR spectra of the S_2 state of PSII + 5% (v/v) (left) and 0.5% (v/v) (right) ^{13}C methanol. Traces in black represent spectra collected at three different tau values—800, 500, and 300 ns—from top to bottom, respectively. Red traces represent spectral simulations at each tau using parameters in Table 1. Experimental data have been smoothed with a 10-point Savitsky–Golay filter. Acquisition parameters: temperature = 4.5 K; ν_{MW} = 34.004 GHz; B_0 = 1227 mT (g = 1.98); $\pi/2_{MW}$ = 12 ns; π_{RF} = 20 μs; srt = 5 ms.

Author Manuscript Author Manuscript Author Manuscript Author Manuscript

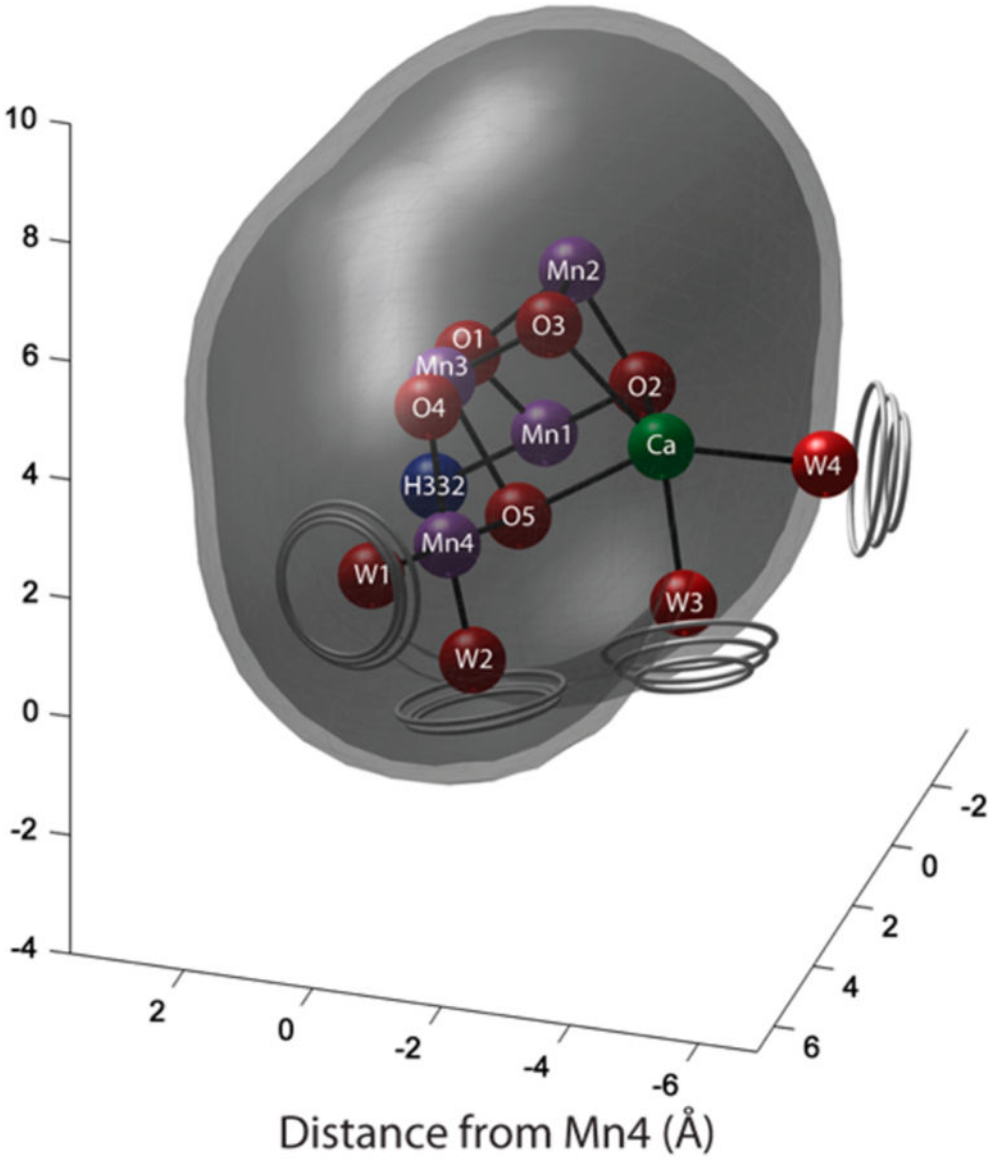

Figure 8.

Dipolar isosurface plot representing the possible position of the methyl ^{13}C nucleus magnetically coupled to the S_2 state of the OEC. Inner and outer dark gray surfaces were calculated using the upper and lower limits of previously published isotropic Mn projection factors (see Table 2) and measured ^{13}C dipolar HFI (see Table 1). Light gray rings are radial distributions of probable locations of the methyl carbon of methanol bound in place of each of the four ligand waters identified in the most recent high resolution crystal structure using bond angles and distances from published crystal structures of synthetic molecules with methanol bound directly to Ca or Mn with the longest, average, and shortest metal–carbon distances for Ca and Mn, respectively.

Author Manuscript Author Manuscript Author Manuscript Author Manuscript

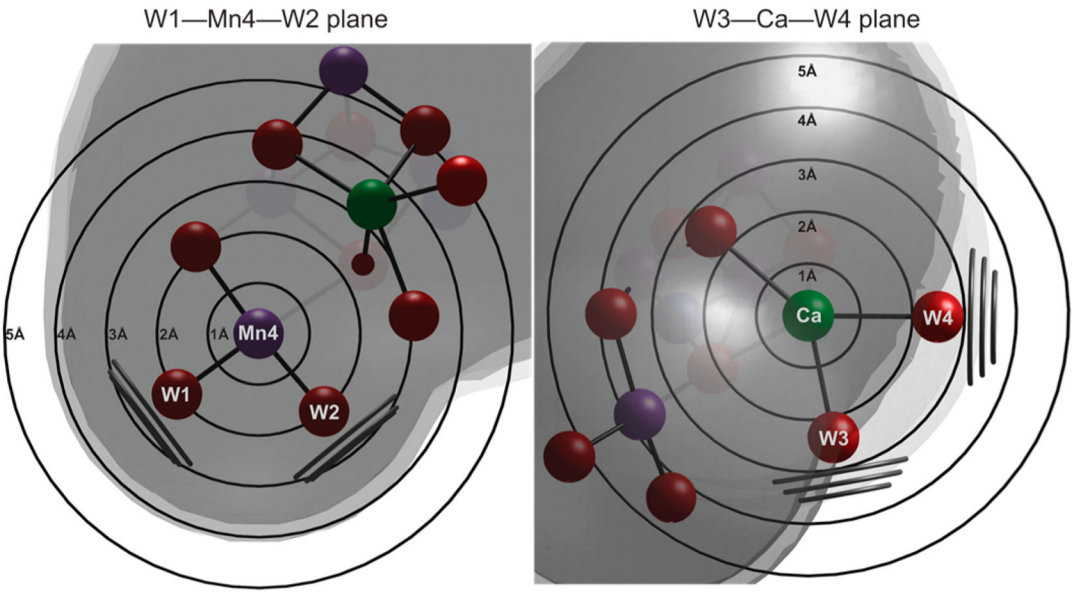

Figure 9.

Plane slices of dipolar isosurface plots from Figure 8 showing the possible position of the methyl ^{13}C nucleus magnetically coupled to the S_2 state of the OEC. Inner and outer gray contours were calculated using the upper and lower limits of previously published isotropic Mn projection factors (see Table 2) and measured ^{13}C dipolar HFI (see Table 1). Black rings denote distance from the Mn_4 and Ca in angstroms. Light gray rings are radial distributions of probable locations of the methyl carbon of methanol bound in place of each of the four ligand waters identified in the most recent high resolution crystal structure using bond angles and distances from published crystal structures of synthetic molecules with methanol bound directly to Ca or Mn with the longest, average, and shortest metal–carbon distances for Ca and Mn, respectively.

Author Manuscript Author Manuscript Author Manuscript Author Manuscript

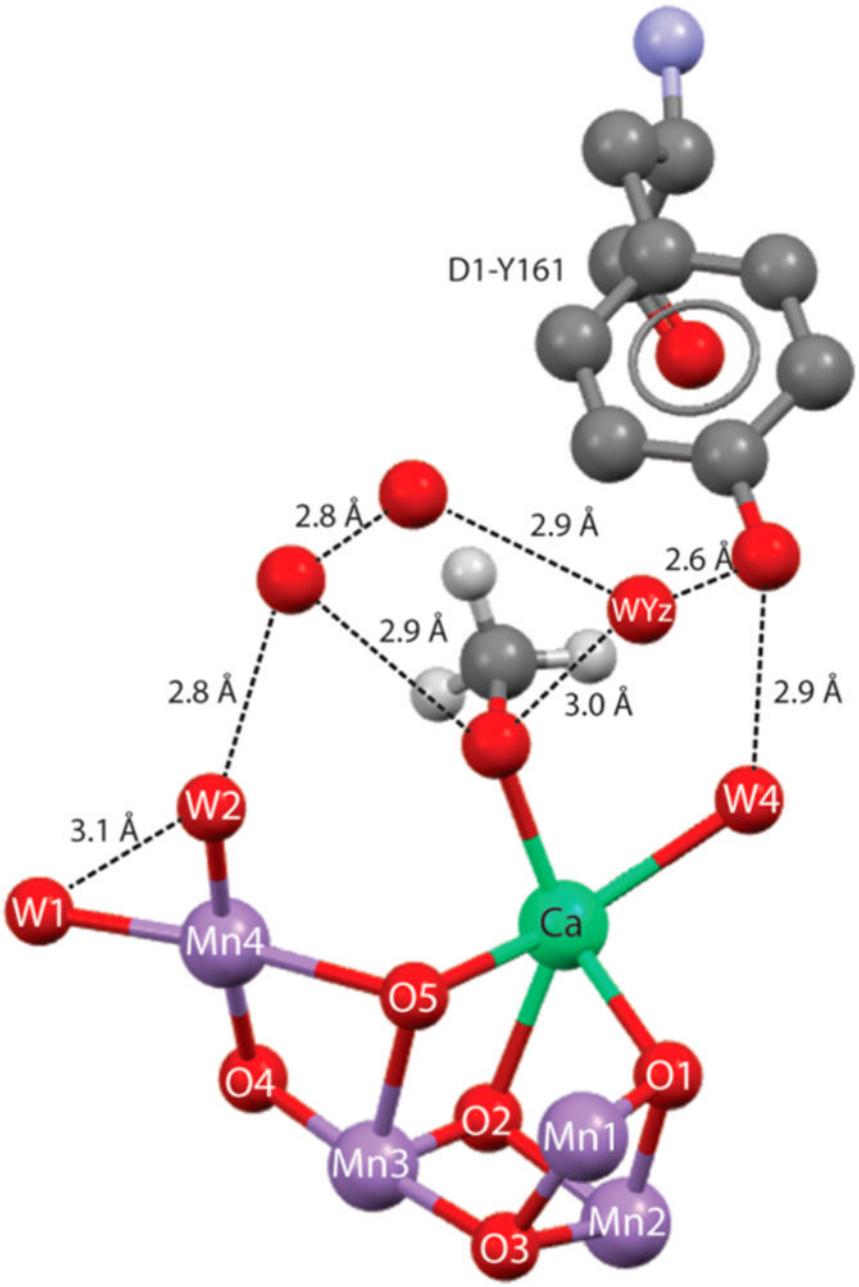

Figure 10.

Model of hydrogen bonding network around the OEC and Y_z with methanol superimposed in place of W3.

Author Manuscript Author Manuscript Author Manuscript Author Manuscript

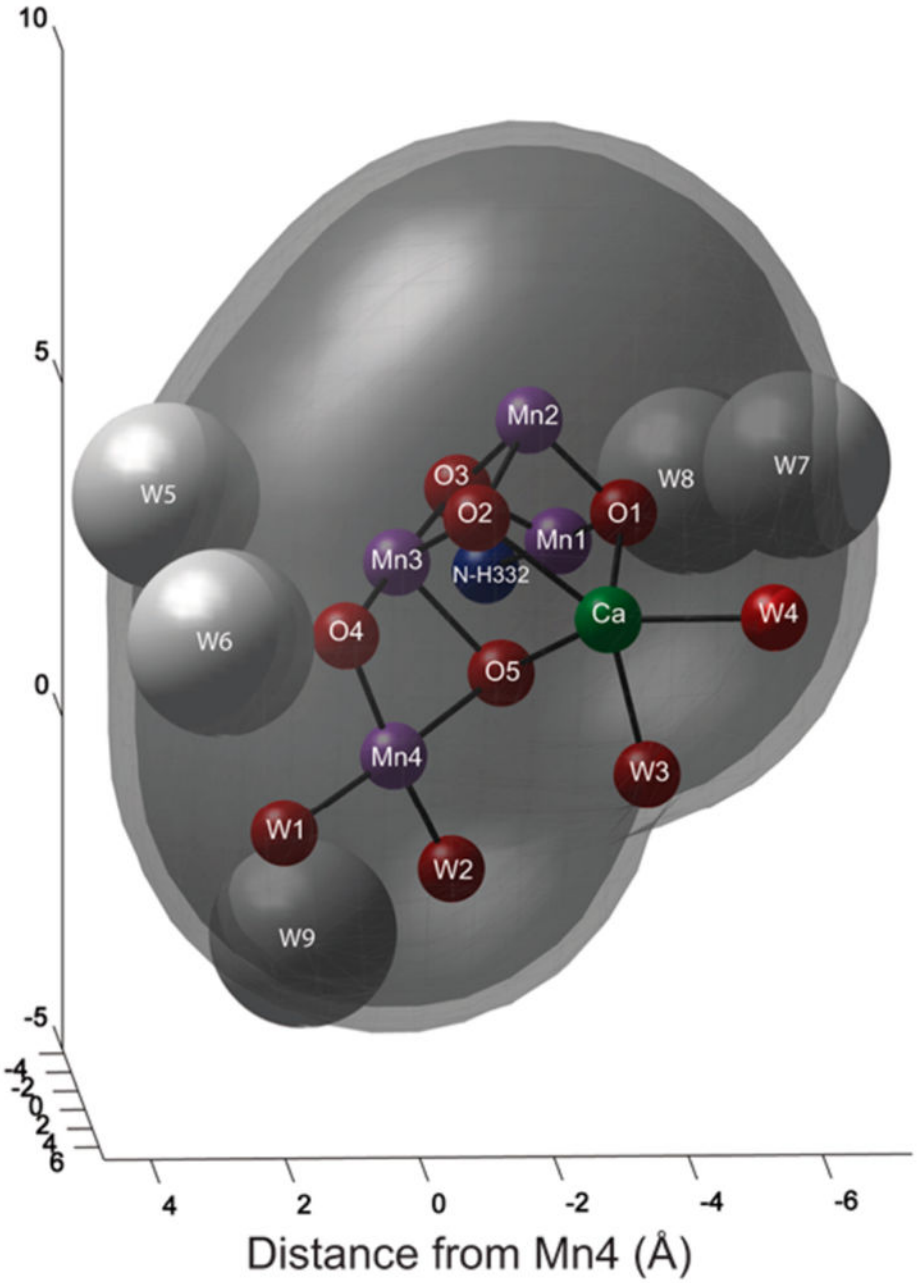

Figure 11.

^{13}C Dipolar HFI isosurface plot representing possible position of the methyl ^{13}C nucleus magnetically coupled to the S_2 state of the OEC. Inner and outer dark gray surfaces were calculated using the upper and lower limits of previously published Mn projection factors and the observed ^{13}C dipolar HFI (see Table 1). Light gray spheres represent isosurfaces 1.4 Å about the oxygen atoms of matrix waters within 5 Å of the OEC evident in the 1.9 Å crystal structure.

Author Manuscript Author Manuscript Author Manuscript Author Manuscript

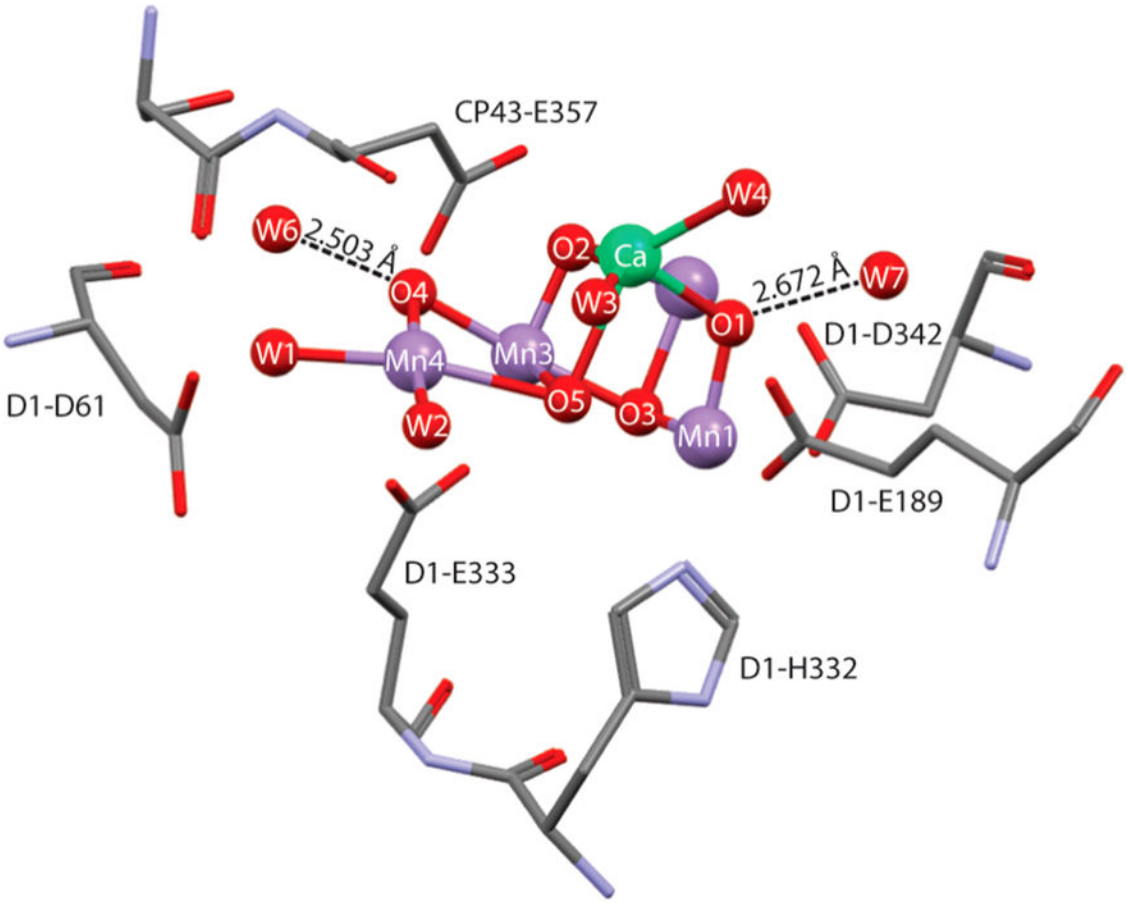

Figure 12.

Matrix waters, W6 and W7, that are likely to participate in hydrogen bonds directly with the Mn_4CaO_5 cluster.

Author Manuscript

Author Manuscript

Author Manuscript

Author Manuscript

Table 1

^{13}C MeOH Magnetic Coupling Parameters[a]

species	A_{iso} (MHz)	T (MHz)
PSII – S_2	0.05 ± 0.02	0.27 ± 0.05
Mn(III,IV)salpn bound MeOH	0.65 ± 0.05	1.25 ± 0.05
Mn(III,IV)salpn matrix MeOH	0.03 ± 0.02	0.12 ± 0.04

[a]HFI tensors assumed to be collinear with g-tensors.

Author Manuscript Author Manuscript Author Manuscript Author Manuscript

Table 2

S_2 MLS Isotropic Mn Spin Projection Factors from Previously Published Experimental Measurements[11] and BS-DFT Calculations[79]

	Mn1(III)	Mn2(IV)	Mn3(IV)	Mn4(IV)	ref
^{55}Mn $\lvert A_{iso}\rvert$ (MHz)	298	248	205	193	11
ρ_{iso} lower limit	1.32	−0.98	−0.81	0.76	
ρ_{iso} upper limit	1.81	−1.33	−1.10	1.03	
BS-DFT ρ_{iso}	1.81	−1.00	−0.93	1.11	79